EPSC2017

TP1 abstracts

EPSC Abstracts
Vol. 11, EPSC2017-15, 2017
European Planetary Science Congress 2017

The role of Late Veneer impacts in the evolution of Venus

C. Gillmann (1), G. Golabek (2), P. Tackley (3) and S. Raymond (4)
(1) Royal Observatory of Belgium, Belgium, (2) University of Bayreuth, Germany, (3) ETH Zürich, Switzerland, (4) Laboratoire d'Astrophysique de Bordeaux (cedric.gillmann@observatoire.be)

Abstract

Our main interest is to understand how different mechanisms contribute to changes in long term evolution. In particular, the primitive history (the first Gy) of terrestrial planets is heavily influenced by collisions. We investigate how the coupled evolution of Venus' atmosphere and mantle is modified by those impacts. We focus on volatile fluxes: atmospheric escape and mantle degassing. We link those processes into a coupled model of mantle convection and atmospheric evolution. Feedback of the atmosphere on the mantle is included. As large impacts are capable of contributing to atmospheric escape, volatile replenishment and energy transfer, we estimate their effects on the evolution of Venus.

1. Introduction

Meteoritic impacts are instant processes that have lasting effects on the long term evolution of terrestrial planets. Collisions affect both the solid part of the planet and its atmosphere in complex ways that need to be quantified. The study of surface conditions and what makes a planet habitable is especially sensitive to small variations and requires a more complete modeling of interactions than parameterized models are able to provide.

1.1 General Model

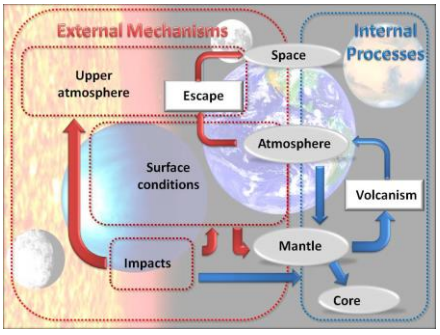

Figure 1: basic layout of the model.

(i) Internal processes are dependent on mantle dynamics. We use a variation of the StagYY code designed for Venus [1]. Physical are depth-dependent. The phase transitions in the olivine system and in the pyroxene-garnet system are included. The assumed rheology is Newtonian diffusion creep plus plastic yielding. Degassing is calculated when melting occurs and we use a wide range of possible lava compositions.

(ii) Atmospheric escape modeling involves two different aspects: hydrodynamic escape (0-500 Myr) and non-thermal escape mechanisms (dominant post 4 Ga). Hydrodynamic escape is the massive outflow of light volatiles into space occurring when solar Extreme UV is strong. Post 4 Ga escape from non-thermal processes is comparatively low. Mechanisms include sputtering, ion pick-up, plasma clouds and dissociative recombination. Constraints include present-day measurements by the ASPERA instrument and numerical simulations.

(iii) Surface conditions are calculated from the greenhouse effect of main gases from the atmosphere: water and CO_2. We use a one-dimensional radiative-convective grey atmosphere model modified from [2]. Surface temperature is calculated and used as a boundary condition for the mantle, creating a feedback between mantle and the atmosphere.

1.2 Impacts

Impacts have three main effects on terrestrial planets. They can (i) bring volatiles and (ii) erode the atmosphere. Volatile deposition assumes chondritic composition and is limited by the fraction of the projectile that is not accreted or that doesn't melt. Atmosphere erosion is inferred using [3]. Mantle dynamics can also be modified by the (iii) large amount of energy brought to the mantle. A thermal anomaly is created by the impact in the mantle and can lead to melting. Collision scenarios are chosen from average and extreme numerical simulations of the Late Veneer period.

2. Results

We are able to produce simulations that are consistent with current Venus situation (atmosphere, resurfacing, volatiles, fractionation). Results linked to present-day atmosphere state are heavily dependent on escape rate and initial volatile inventory. Surface conditions depend mainly on atmosphere water content. Surface temperature has a direct influence on mantle convection with low temperatures correlated with mobile lid behavior while high ones favor stagnant or episodic lid. Mobile-lid regime is akin to plate tectonics and could be a way to inject volatiles back into the mantle.

Large impacts are shown to affect only marginally the evolution of Venus through atmosphere erosion. Single impacts don't have enough eroding power to durably affect the atmosphere and large impacts are not numerous enough. Swarms of small bodies (<50km radius) might be a better candidate for this process. Large impacts actually bring more volatiles than they blow off, at all compositions tested (fig.2).

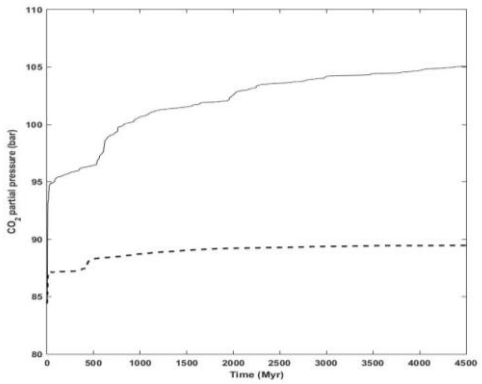

Figure 2: CO2 pressure evolution of the atmosphere of Venus. Impact delivery is taken into account for two projectile compositions: ordinary chondrite (dashed line) and carbonaceous chondrite (full line).

The amount of volatiles brought by large impactors is comparable to the amount of degassing taking place during the subsequent evolution. This occurs very early in the history of the planet and affects initial conditions of the simulations. As a volatile source, it is opposed by the high escape fluxes of early evolution (hydrodynamic escape).

A second important effect of large collisions is the thermal anomalies thus produced. When impactors are bigger than 200-300 km radius, they start to affect a deep enough portion of the mantle to have long term consequences. Anomalies tend to propagate by spreading across the surface due to the buoyancy of the hot material. Old crust is destroyed or remixed in the mantle. Impacts lead to the melting of a large part of the upper mantle leading to its depletion (fig. 3) and degassing. As we consider no process that remixes volatiles into the mantle, with enough large impacts distributed over the planet, the mantle can be efficiently depleted by more than 90% of its volatiles in the first few tens to hundreds of million years. This drastically cuts down degassing in the late history of the planet and leads to lower present-day surface temperatures.

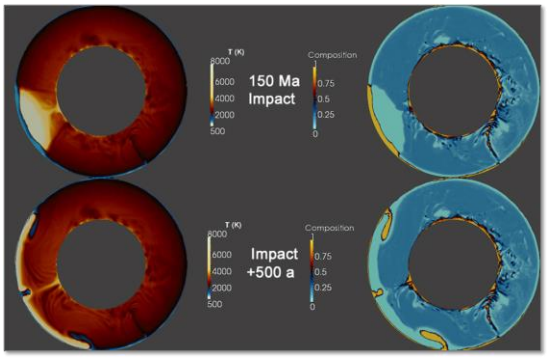

Figure 3: Mantle temperature and composition fields after a large (800km) impact. Upper mantle is mobilized and depleted.

3. Summary and Conclusions

Late Veneer impacts heavily affect initial conditions of terrestrial planets evolution, in particular regarding the volatile inventory. While they do not cause much atmosphere erosion, they release large amounts of gases and lead to widespread degassing. They can also efficiently deplete the mantle of the planet. In order to better constrain planetary evolution, it becomes essential to assess the recycling of volatiles into the mantle both during impacts and afterwards (during periods of mobile lid regime, for example).

References

[1] Armann, M., and P. J. Tackley, Simulating the thermochemical magmatic and tectonic evolution of Venus's mantle and lithosphere: Two-dimensional models, J. Geophys. Res., 2012.

[2] Phillips, R.J., et al. Climate and interior coupled evolution on Venus. Geophys. Res. Lett. 28, 2001.

[3] Shuvalov, V., 2009. Atmospheric erosion induced by oblique impacts. Meteorit. Planet. Sci. 44, 1095–1105.

EPSC Abstracts
Vol. 11, EPSC2017-34, 2017
European Planetary Science Congress 2017

Orbital energy – a main source of structuring force for celestial bodies

G.G. Kochemasov
IGEM of the Russian Academy of Sciences, 35 Staromonetny, 119017 Moscow, RF,
kochem.36@mail.ru

The classical planetology considers impacts as a main source of energy reworking surfaces and partly the deeper spheres of celestial bodies. However a region or regions of origin of impacting objects affecting all without exception planetary bodies in all parts of the Solar system is poorly understood. At the same time planetologists now have several tens of images of full discs of these bodies. Distribution patterns of "impact traces" – craters in many of them are surprisingly regular. They show alignments, regular grids not related to random hits expected from impacts but rather require more regular and ubiquitous structuring force. Moreover, such regular patterns appear in the outer gaseous spheres of some bodies including the Sun's photosphere (Fig. 1).

It was shown earlier (Kochemasov, 1995-2013) [1, 2] that such regular patterns appear due to warping action of inertia-gravity waves affecting all bodies moving in keplerian elliptical orbits (Fig. 2). Periodically changing accelerations of celestial bodies cause their wave warping having in rotating bodies (but all bodies rotate!) four ortho- and diagonal directions. An interference of 4 directions of standing waves brings about a regular net of uprising, subsiding and neutral tectonic blocks. Naturally polygonal in details they appear as rings in cosmic images. This is one of reasons why they are often confused with round impact craters and essentially disfigure their statistics.

A fundamental nature of the wave woven nets of even sized round "craters" (granules) is dependence of the "crater" sizes on orbital frequencies of bodies. The lower frequency the larger size, the higher frequency the smaller granule sizes. One could compare 5 bodies with widely differing orbital frequencies, sizes and compositions: Titan (1/15.94days), Callisto (1/16.69), Moon (1/27.32), Mercury (1/87.97), Earth (1/365.3). Moon (1/27.32), Mercury (1/87.97), Earth (1/365.3). Images of their discs "peppered" with round features diameters of which precisely correspond to their orbital frequencies witness that such tectonic patterns can originate due to orbital energies. "Orbits make structures" – this short notion adequately reflects the expressed above observations (Fig. 1).

The existing correspondence between orbital frequencies and tectonic granulations proving the structuring role of orbital energy was earlier noted in comparative planetology of the terrestrial planets. The row of Mercury, Venus, Earth, Mars, and asteroids with decreasing orbital frequencies is remarkable by increasing relative sizes of tectonic granules, relief ranges, iron content in lowland basalts and decreasing atmospheric masses from Venus to Mars.

In summary, firmly established tectonically identical structural features observed in cosmic bodies of various classes, sizes, compositions (Fig. 1) underline important role of external structuring energy. It presents itself as the orbital mechanical energy. In full consent with the classical physics the mechanical energy transfers into heat energy of cosmic bodies influencing their tectonics. That is why extremely frozen and small body as Pluto has comparable tectonic structures with large full of inner energy planets as Earth. Recently appeared paper [3] shows comparable tectonic structures in Earth and Moon, Earth and Mercury.

[1] Kochemasov, G.G., 1998. Tectonic dichotomy, sectoring and granulation of Earth and other celestial bodies. Proceedings of the International Symposium on New Concepts in Global Tectonics, "NCGT-98 TSUKUBA", Geological Survey of Japan, Tsukuba, Nov 20-23, 1998,144-147. **[2]** Kochemasov, G.G., 1999. Theorems of wave planetary tectonics. Geophys. Res. Abstr., v.1, no. 3, p. 700. **[3]** Kochemasov G.G. New planetology and geology: tectonic identity and principal difference of terrestrial oceans and lunar basins // New Concepts in Global Tectonics (NCGT) Journal, 2017, V. 5, # 1, p 131-133.

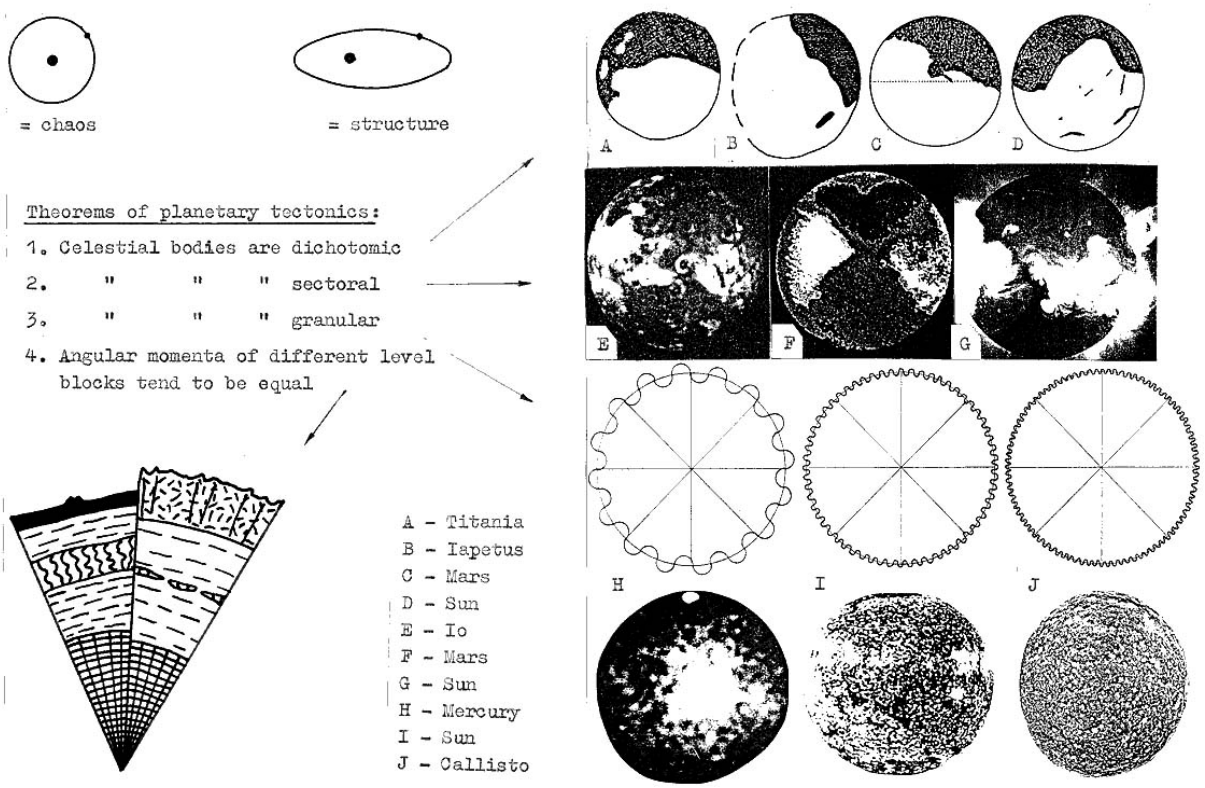

Fig. 1. Wave woven tectonic segments, sectors, and granules in cosmic bodies of various sizes, states, and compositions [1].

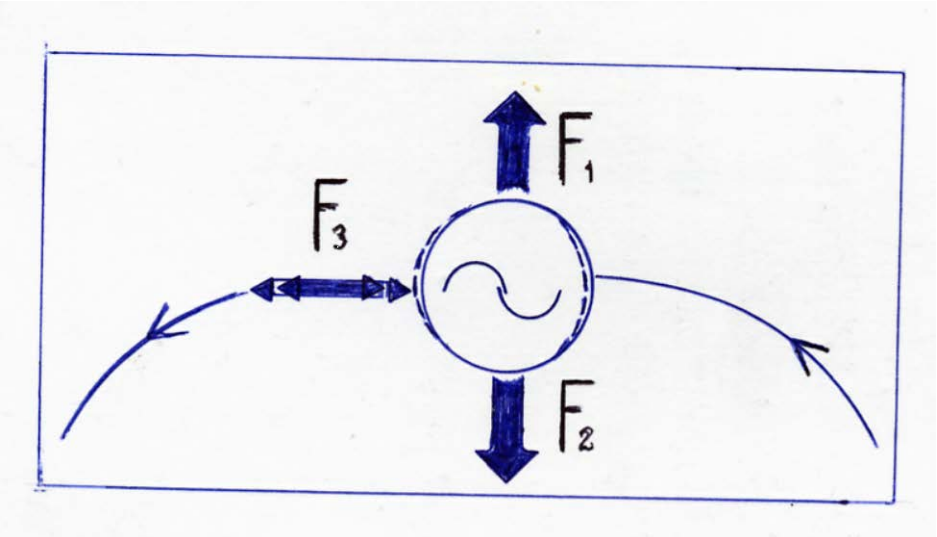

Fig. 2. Forces acting upon a celestial body moving in an elliptical keplerian orbit. F1-centrifugal, F2-gravity, F3-varying orbital force making a body to oscillate and produce structures (Fig. 1).

EPSC Abstracts
Vol. 11, EPSC2017-38, 2017
European Planetary Science Congress 2017

Global degassing leading to formation in crust of hydrocarbon concentrations and kimberlites

G. Kochemasov, IGEM of the Russian Academy of Sciences, 35 Staromonetny, 119017 Moscow, RF, kochem.36@mail.ru

"Orbits make structures" – a main point of the new wave planetology based on one important property of the Keplerian elliptical planetary orbits. The ellipticity implies periodical changes of accelerations and, thus, orbital forces structuring cosmic bodies. The Earth and the Moon sharing the same circumsolar orbit have similar main structural features. Among them there are terrestrial Oceans and lunar Basins. The most obvious are two tectonic triads: Pacific Ocean – Malay Archipelago – Indian Ocean on Earth and Procellarum Basin – Mare Orientale – SPA Basin on the Moon. The planetary depressions of both bodies are covered with basalts, but basaltic effusions are drastically different in age: the AR on Moon and Mz-Cz on Earth. These ages well correlate with the body masses. The more massive and inert Earth has heated and melted mantle much later (The Newton's law of inertia). Energy of movement transfers to the heat energy.

The Earth and Moon's subsided hemispheres, for keeping angular momenta of hemispheres equal, are filled with dense basaltic material. But times of the fillings are significantly different. The Earth-Moon system expands with time. This means increasing its angular momentum. A natural response to it is in slowing down rotation of both bodies diminishing their angular momentum (action - opposite action). Diminishing momenta are compensated by melting and uplifting to surfaces dense basaltic material [1]. But on the Moon it happened much earlier (4.5-3 billion years ago) because of diminished inertia of the small mass satellite. At Earth - much larger and massive body than Moon – 81 times – it happened much later. (3-4.5 billions): 81 = 37-55 million years. According to this calculation, a "peak" of the basaltic reaction of Earth, filling in by basalts of oceanic depressions is in the boundary of Mesozoic and Cenozoic.

Enormous heating of terrestrial lithosphere documented by thick planetary wide asthenosphere (stable and thick in oceanic tectonic blocks) leads to massive liberation (release) of volatiles, among them H2, CH4, N2. They penetrate in the upper solid geosphere making large concentrations of hydrocarbons in form of conventional deposits in "voids" and occurrences in slates and oceanic bottom ices. Ages of hydrocarbon deposits are mainly Mesozoic (70% Mesozoic in age, 20% Cenozoic, 10%Paleozoic) and well agree with the episode of global heating and effusions of oceanic basalts [1]. These events are not occasional but tied causatively. This means that origin of hydrocarbon deposits is mainly inorganic though some decomposition of organic matter in sedimentary rocks also exists. Flux of volatiles could accelerate the organic decay.

Another unexpected coincidence of the global heating, basalt "explosion", hydrocarbon concentrations and kimberlite magmatism is evident and impressive. Thick "roots" of Archean cratons , massive lithosphere help to keep certain volumes of volatiles strongly pressed. Overcoming enormous pressure of the upper lithosphere strongly squeezed fluids ("fluidizites", according to Prof. A.M. Portnov) find way up using narrow cracks. Reaching upper predominantly sedimentary layers with small pressure the fluids explode making kimberlite "cones", pipes. Methane, meeting oxygen, burns to CO2 and H2O producing usual in kimberlites serpentines. In some very rare cases (3 to 5 % of kimberlite pipes) carbon is not burned totally and precipitates as crystalline substance – diamond. Normally it keeps ideal angular shapes proving that it do not suffered long hard way out of the mantle –asthenosphere (other hard minerals often are rounded). Diamond age normally judged by seized inclusions is much older than kimberlites, but actually it is comparable to the host kimberlites. Now the low pressure and very transparent diamonds are obtained from vapor in experiments [3]. Many years ago Prof. A.M. Portnov proposed and substantiated this way to origin of natural kimberlites and diamonds [2].

References:

[1] Kochemasov G.G. New planetology and geology: tectonic identity and principal difference of terrestrial oceans and lunar basins // New Concepts in Global Tectonics (NCGT) Journal, 2017, V. 5, # 1, p 131-133.

[2] Portnov A.M. . Secrets of origin of diamond and gold deposits // Industrial registers, # 7-8, July-August 2012. (In Russian)

[3] Meng Yu-fei, Yan Chih-shine, Krasnicki S…..Hemley R.J. High optical quality multicarat single crystal diamond produced by chemical vapor deposition // Physica status solidi (a), v. 209, Issue 1, p. 101-104, January 2012. DOI: 10.1002/pssa.201127417

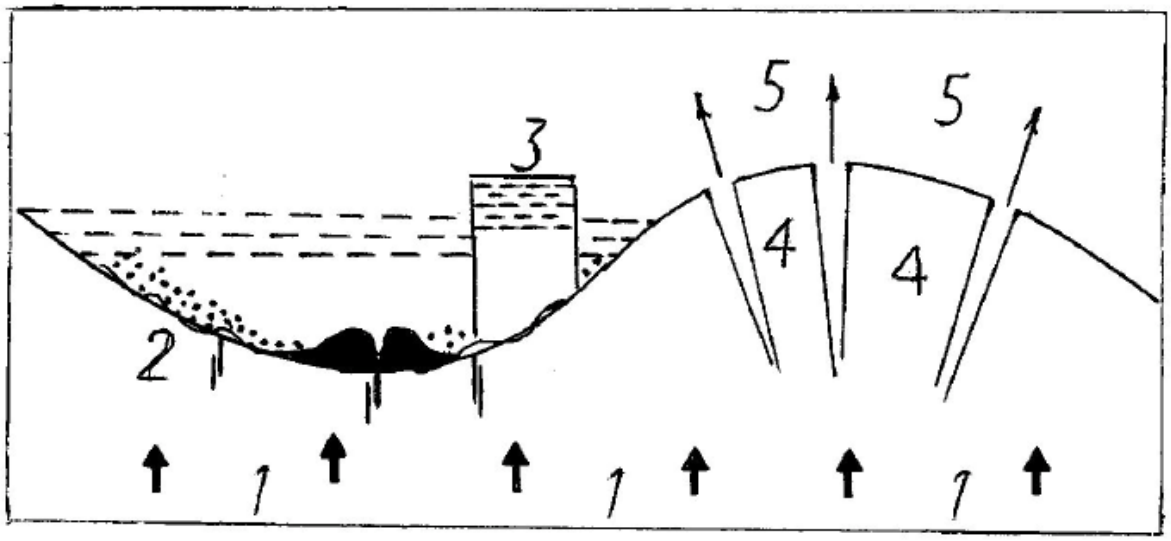

FIG. 1. Scheme of hydrocarbon degassing of Earth (1) with a principal difference between uplifted an subsided tectonic blocks (for the fundamental wave these are two hemispheres-segments). 2- crumpling and faulting, "squeezing" basalts in middle-ocean ridges, gashydrate formation (points). 3- uplifted continents of the subsided hemisphere with "slate barriers" on continents impregnated by slate gases an light oil. 4- broken by cracks-rifts uplifted block enriched with less movable liquid hydrocarbons as a result of intensive degassing (5).

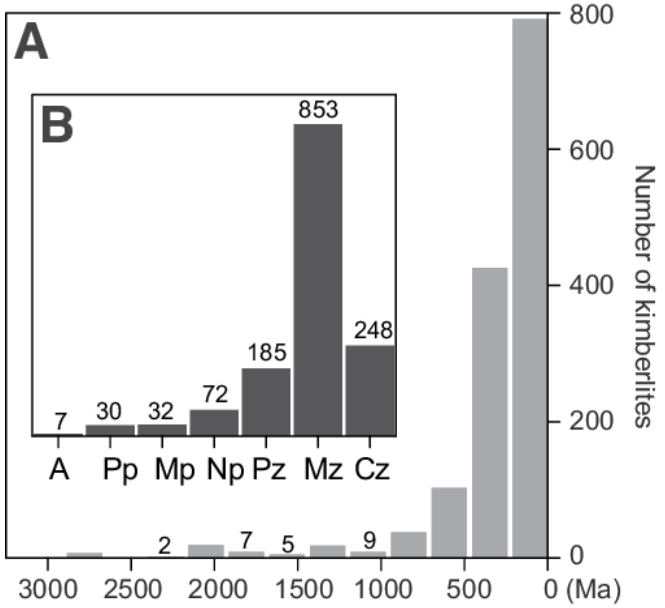

Fig. 2. Histogram of kimberlite ages based on the compilation of Faure, 2006-A-Ages.

EPSC Abstracts
Vol. 11, EPSC2017-68-1, 2017
European Planetary Science Congress 2017

Refining the boundary between the Phobos Blue/Red spectral units with the ExoMars-CaSSIS imagery

M. Pajola (1,2), E. Simioni (3,2), A. Lucchetti (2), C. Re (2), G. Cremonese (2), N. Thomas (4), A. Pommerol (4), L. Tornabene (5) and the CaSSIS Team
(1) NASA Ames Research Center, Moffett Field, CA 94035, USA (maurizio.pajola@nasa.gov, maurizio.pajola@gmail.com) (2) INAF Osservatorio Astronomico di Padova, 35122 Padova, Italy, (3) CNR-IFN UOS Padova LUXOR, Padova, Italy (4) Physikalisches Institut der Universität Bern, 3012 Bern, Switzerland, (5) Centre for Planetary Science and Exploration, Department of Earth Sciences, University of Western Ontario, London, Ontario N6A 5B7, Canada

Abstract

The Martian satellite Phobos has been the subject of several photometric and spectroscopic studies ranging from the Visible to the Infrared wavelength range over the past 40 years [1]. In particular, disc-resolved observations of the leading and trailing parts of the anti-Mars hemisphere of the satellite and part of the sub-Mars hemisphere were obtained with the Videospectrometric Camera (VSK), the Combined Radiometer and Photometer for Mars (KRFM), and the Imaging Spectrometer for Mars (ISM) on 1989 USSR Phobos 2 mission. By means of these observations the spectral characteristics of specific areas were investigated, and it was determined that Phobos could be divided into two main spectral units, i.e. the so-called “bluer” and “redder” unit [2]. High-resolution colour imaging by the HiRISE instrument on Mars Reconnaissance Orbiter shows that the bluer unit appears to drape over the rim of Stickney. Bluer material can be seen both inside and outside the crater rim [3]. Over the following years multiple works have attempted to understand whether this spectral dichotomy is due to different mineralogical compositions, surficial grain sizes or the extent of space weathering. However, this aspect remains a matter of debate [4-8], and thus requires additional data analysis. Furthermore, sample return missions targeting Phobos are being proposed to improve our understanding of these spectral characteristics. An example is the JAXA Mars Moon eXploration (MMX) mission, which has been accepted as the next Japanese flagship mission. The intention is to return samples taken from both the bluer and the redder units by 2029 (http://mmx.isas.jaxa.jp/en/index.html).

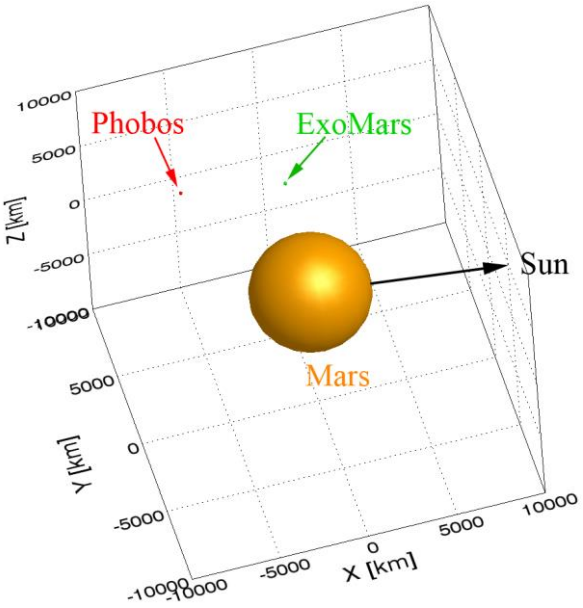

Fig. 1: The geometry of ExoMars-Phobos observation. The black arrow points towards the Sun.

On 26 November 2016, the ESA ExoMars Trace Gas Orbiter performed a close approach to Phobos at a distance of ~7600 km. The geometry of the observation (Fig. 1) allowed the Colour and Stereo Surface Imaging System (CaSSIS, [9]) instrument to capture a stereo pair centred on the boundary of the two spectral units in the direction of the sub-Mars point. This study focuses on this image pair in order to refine the distribution and spatial extent of the two units, and to provide detailed colour maps that can be used by the future MMX mission in order to select the Phobos sampling sites.

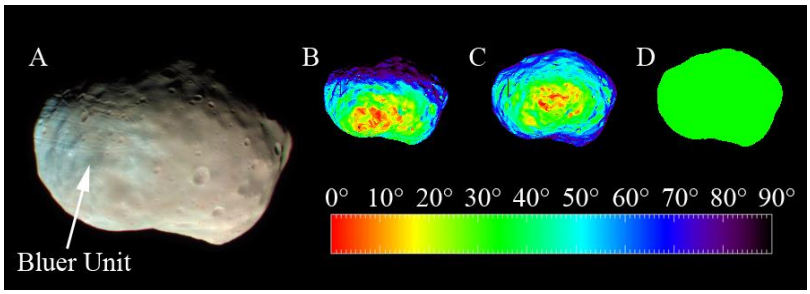

Fig. 2: A) RGB image prepared using filters at 0.937 μm for Red, 0.675 μm for Green and 0.499 μm for Blue. The Bluer unit is indicated as well. B, C and D are the incidence map, the emission map and the mean phase angle (35°) map, respectively.

CaSSIS images in four different filters: BLU – 0.499, PAN – 0.675, RED – 0.836 and NIR – 0.937 μm, [9]. The CaSSIS image was obtained when Phobos was on the dark side of Mars, so there is little or no Mars shine affecting the dataset. The spatial resolution is ~ 85 m (Fig. 2). The images were mosaicked with a recursive process using the Speeded Up Robust Features (SURF). The photometric incidence (i), emission (e) and mean phase angle (α) maps related to the CaSSIS observation were calculated from the 3D shape model of [10] by using the SPICE kernels ExoMars-Phobos geometric information [11]. We then computed the Lommel-Seeliger disk function (D(i,e)) for each CaSSIS Phobos pixel and corrected the datacube by dividing the I/F of each pixel by these values. In the photometrically corrected cube, the regions with angles larger than 80° are excluded.

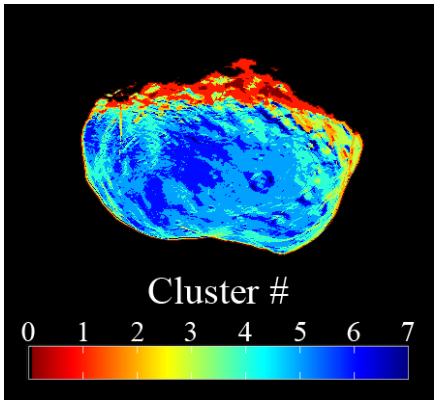

Fig. 3: The clusters identified on the CaSSIS dataset.

In order to refine the boundary between the spectral bluer and the redder unit we applied on the 4-filters dataset a statistical clustering based on a K-means partitioning algorithm [12]. It was developed and evaluated by [12,13] and makes use of the Calinski and Harabasz criterion [14] to find the intrinsically natural number of clusters, making the process unsupervised. A natural number of eight clusters was identified within the CaSSIS cube, see Fig. 3. Each resulting cluster is characterized by an average spectrum and its associated variability: Cluster #6 is the one with the flatter spectral trend and represents the bluer unit observed in Fig. 2A. All other clusters have spectra with distinct redder slopes. The geographical location of the bluer unit we obtained has then been reprojected on Phobos 3D shape model, and 3D maps available for the MMX mission are eventually prepared.

Acknowledgements

M.P. was supported for this research by an appointment to the National Aeronautics and Space Administration (NASA) Post-doctoral Program at the Ames Research Center administered by Universities Space Research Association (USRA) through a contract with NASA. The authors wish to thank the spacecraft and instrument engineering teams for the successful completion of the instrument. CaSSIS is a project of the University of Bern and funded through the Swiss Space Office via ESA's PRODEX programme. The instrument hardware development was also supported by the Italian Sace Agency (ASI) (ASI-INAF agreement no.I/018/12/0), INAF/Astronomical Observatory of Padova, and the Space Research Center (CBK) in Warsaw. Support from SGF (Budapest), the University of Arizona (Lunar and Planetary Lab.) and NASA are also gratefully acknowledged.

References

[1] Duxbury, T.C. et al., 2014. *Planet. Space Sci.* 102, 9. [2] Murchie S., Erard S., 1996, *Icarus*, 123, 63. [3] Thomas, N. et al., 2011. *Planet. Space Sci.* 59, 1281. [4] Gondet B. et al. EPSC 2010 p. 548. [5] Pajola, M. et al., 2012. *Mon. Not. R. Astron. Soc.* 427, 3230. [6] Fraeman, A.A. et al., 2014. *Icarus* 229, 196. [7] Pajola, M. et al., 2013. *Astrophys. J.* 777 (2), 127. [8] Witasse, O. et al., 2014. *Planet. Space Sci.* 102, 18. [9] Thomas, N. et al., 2016. 47th LPSC, Abstract # 1306. [10] Gaskell, R.W. 2013, NASA PDS. [11] Acton, C. H. 1996, *Planet. Space Sci.*, 44, 65. [12] Marzo, G. et al. 2009, *JGR*, 114, E08001. [13] Marzo, G. et al. (2008), *JGR*, 113, E12009. [14] Calinski, T., Harabasz, J., (1974), *Commun. Statist.* 3, 1.

EPSC Abstracts
Vol. 11, EPSC2017-69, 2017
European Planetary Science Congress 2017

Modelling the Phobos MRO/CRISM dataset in the 0.5-2.5 µm range with multiple optical constants

M. Pajola (1,2), T. Roush (2), C. Dalle Ore (2,3), G. A. Marzo (4) and E. Simioni (5)
(1) Universities Space Research Association, NASA NPP Program (Supported by an appointment at NASA Ames Research Center: maurizio.pajola@nasa.gov), (2) NASA Ames Research Center, Moffett Field, CA 94035, USA, (3) Carl Sagan Center, SETI Institute, Mountain View, CA 94043, USA (4) ENEA Centro Ricerche Casaccia, 00123 Roma, Italy (5) INAF Osservatorio Astronomico di Padova, 35122 Padova, Italy.

Abstract

The Phobos origin remains the subject of scientific discussion. There is no definitive evidence if it is a captured asteroid or if it formed in situ around Mars. Recently, the JAXA Mars Moon eXploration (MMX) mission has been approved as the next Japanese flagship mission, with the main aim of solving this puzzle by sampling the surface of Phobos and returning the samples back to Earth for analyses by 2029. Nevertheless, before waiting for such important future analysis, the Mars Reconnaissance Orbiter (MRO) CRISM dataset still remains a fundamental means to study Phobos surface mineralogical composition.

We use the CRISM 0.5 – 2.5 µm dataset obtained on 10/23/2007 when Phobos was on the dark side of Mars. The data were obtained with a phase angle of 40° and a scale of 356 m/pixel. The photometric incidence (i) and emission (e) were calculated from the 3D shape model of [1] by using the SPICE kernels MRO-Phobos geometric information [2]. We then computed the Lommel-Seeliger disk function for each CRISM Phobos pixel:

$$D(i,e) = 2\cos(i)/\cos(i)+\cos(e).$$

The CRISM corrected dataset is then obtained by dividing the I/F images by D. In our analyses, the photometrically corrected regions with angles larger than 80° are excluded.

After eliminating the bad pixels and lines we applied a statistical clustering over the entire dataset (0.5-2.5 µm) using a K-means partitioning algorithm previously developed [3] and applied to various data [4, 5]. The algorithm uses the Calinski and Harabasz criterion [6] to find the intrinsically natural number of clusters, making the process unsupervised. A natural number of seven clusters was identified within the CRISM Phobos dataset, as shown in Fig. 1. Each resulting cluster is characterized by an average spectrum (Fig. 2), and its standard deviation.

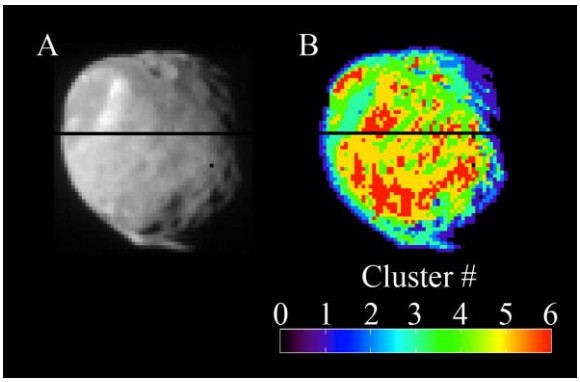

Fig. 1: A) The CRISM original I/F Phobos dataset. B) The seven clustering classes identified by statistical clustering.

This approach has been previously applied for compositional interpretation of different Solar System objects, e.g. asteroids, Mars, Mercury and Iapetus [7, 8, 9, 10]. The algorithm is agnostic of the physical meaning of the resulting clusters, and scientific interpretation is required for their subsequent compositional evaluation.

Shkuratov's model [11] was used for compositional interpretation of Phobos spectra. The model calculates the albedo of a powdered surface from the optical constants of candidate materials. We started the modeling using the materials suggested by Pajola et al. [12] that include Tagish Lake meteorite [TL, 13] and Mg-rich pyroxene glass [PM80, 14].

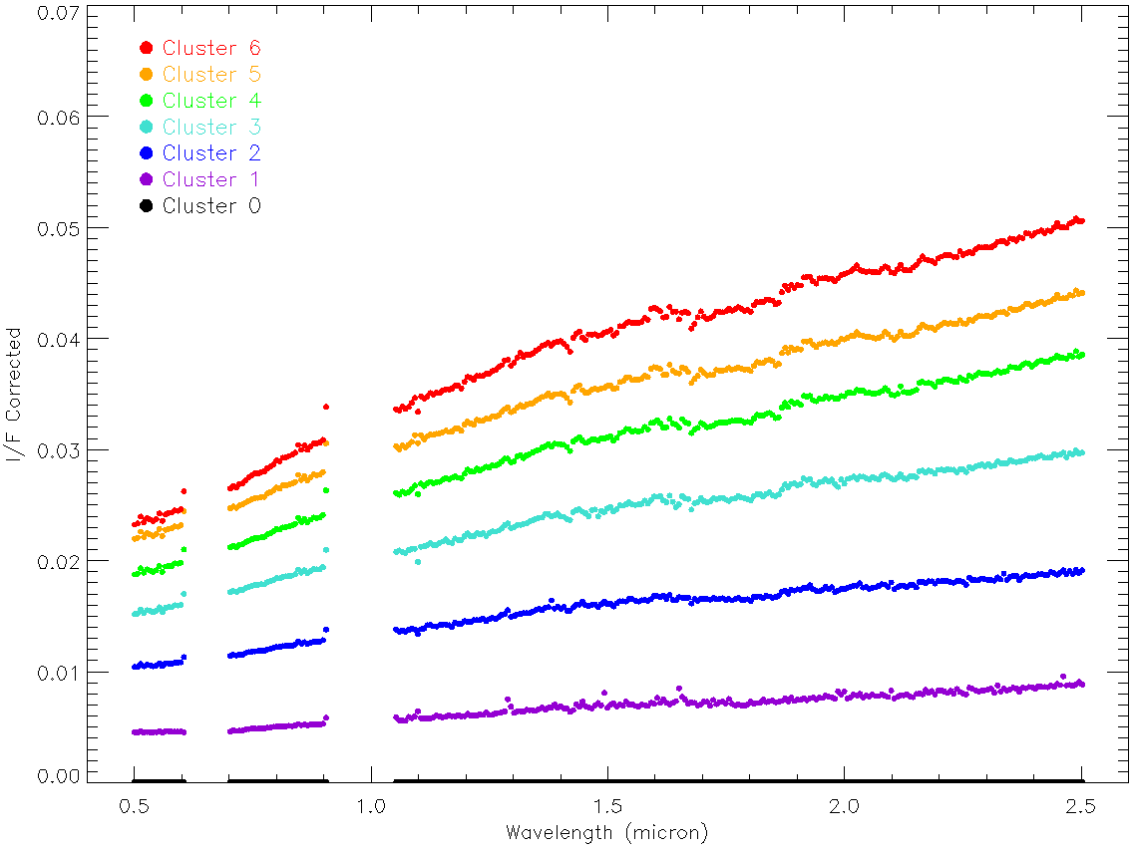

Fig. 2: The mean spectra for each class presented in Fig. 1.

The Shkuratov model is used in a downhill simplex algorithm [15] that iteratively, and simultaneously changes the relative abundance and grain sizes of these two components to minimize the differences between the model and observations using a χ^2 criterion. The best-fitting models were achieved with a simple intimate mixture.

The results obtained for the clusters identified from the statistical analyses will be presented, together with different best-fitting compositions characterized by multiple optical constants.

Acknowledgements

M.P. was supported for this research by an appointment to the National Aeronautics and Space Administration (NASA) Post-doctoral Program at the Ames Research Center administered by Universities Space Research Association (USRA) through a contract with NASA.

References

[1] Gaskell, R.W. (2013) NASA Planetary Data System. [2] Acton Jr, C. H. 1996, *Planet. Space Sci.*, 44, 65. [3] Marzo, G. et al. (2009), *JGR*, 114, E08001. [4] Marzo, G. et al. (2008), *JGR*, 113, E12009. [5] Marzo, G. et al. (2009), *JGR*, 114, E08001. [6] Calinski, T., Harabasz, J., (1974), *Commun. Statist.* 3, 1–27. [7] Marzo, G. et al. (2009), *JGR*, 114, E08001. [8] Lucchetti, A. et al. (2017), 48th LPSC Conference. LPI Contribution No. 1964, id.1329. [9] Pinilla-Alonso, N. et al. (2011), *Icarus*, 215, 1, 75. [10] Dalle Ore, C. et al. (2012), *Icarus*, 221, 2, 735. [11] Shkuratov, Y. et al. (1999), *Icarus*, 137, 235. [12] Pajola, M. et al. (2013), *ApJ*, 777, 127. [13] Roush, T. L. (2003), *Met. & Planetary Science*, 38, 419. [14] Dorschner, J. et al. (1995), *A&A*, 300, 503. [15] Press, W. H. et al. (1992), Cambridge Univ. Press, New York.

EPSC Abstracts
Vol. 11, EPSC2017-117-1, 2017
European Planetary Science Congress 2017

A Tentative Mechanism for Dust Vertical Transport at Extreme Altitudes from the Collapse of Supersaturated Tropospheric Cavities on Mars with Particular Reference to March 2012 Event

Francisco J. Arias[(1)]
[(1)] Department of Fluid Mechanics, University of Catalonia, ESEIAAT C/ Colom 11, 08222 Barcelona, Spain

Abstract

Consideration is given to the formation and collapse of supersaturated tropospheric cavities on Mars for dust vertical transport at extreme altitudes as a tentative mechanism explaining the martian march-2012 plume. It will be shown that if, during the night-time radiative cooling is exacerbated by suspended dust surrounding a tropospheric parcel and then impeding heat flow from the surface into the parcel and if, additionally the parcel itself is devoid of condensation nuclei (dust aerosol on Mars) a supersaturated cavity might be generated. Then, with the first rays of sunlight in the morning -and the beginning of the daily dust activity, any dust incursion into the cavity driven by local winds, could trigger the condensation of the parcel and the subsequent vigorous prompt collapse of the cavity. Utilizing a simplified geometrical model, it is shown that the collapse and rebound of such tropospheric cavities could provide enough energy to lift dust well into the thermosphere and then a possible explanation to the extremely high-altitude plumes seen on Mars. The proposed hypothesis seems consistent with the high-altitude plume seen at Mars 2012 at Cimmeria region -and still unresolved, occurred at the Martian terminator (the day-night boundary) when the atmosphere could be coldest because has been without the heat of the sun for the longest time and the beginning of the dust activity driven by solar heating. Finally the possibility that the local strong magnetic field in Cimmeria region may have played a role in triggering the formation of the hypothesized supersaturated tropospheric cavity or *"magnetocavity"* was also discussed.

Introduction

On 12 March 2012, amateur planetary observers reported an unusual small protrusion seen at sunrise of Mars within the Terra Cimmeria region at roughly 45^o south, 195 ^{o} west. The protrusion became more prominent over the following days until March 23rd. In 2015 a thorough research report undertaken by the Prof. Sanchez-Lavega research group at the Universidad del Pais Vasco, Spain, estimated the height of these plumes as 200 to 250 km above the surface of Mars,[1]. Since then, concern has been raised in the scientific planetary community because according with the general circulation model (GCM) for Mars, [2], clouds should not exist this high in Mars´s atmosphere. The mystery about what happened on 2012 is still unresolved.
From photometric measurements, two possible scenarios were explored in that report in order to explain the event. These two scenarios are as follows:

In the first scenario the observed plume is formed by particle of CO_2-ice, H_2O-ice or dust reflecting solar radiation with a best fit for CO_2-ice, H_2O-ice particles with effective radii of $0.1^{+0.1}_{-0.04}\mu$m. However, according with the general circulation model (GCM) for Mars, H_2O condensation at the relevant altitudes requires either anomalous temperature drop $>$ 50 K or an unusual increase in the H_2O mixing ratio to complete saturation above 140 km. For CO_2 condensation the situation is even worse, requiring temperature drop of 100 K above 125 km. (see Fig. 1). In addition, explaining the plume as formed by dust would require a strong vertical transport up to at least 180 km above the surface. There is only a known mechanism -so far, able to provide the required vigorous updrafts which is driven by dry convection under high insolation called *rocket dust storms*, [3],

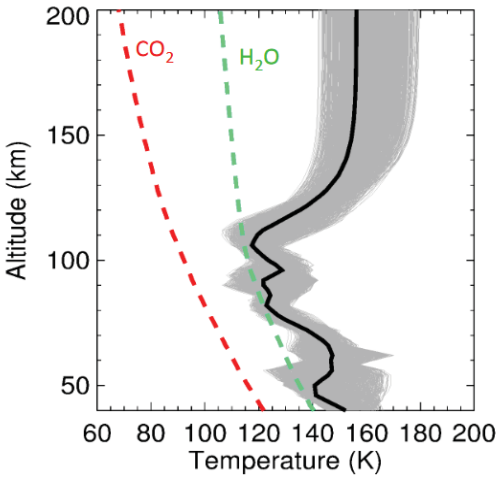

Figure 1: Atmospheric temperature profile and water and carbon dioxide condensation temperatures on Mars. From Sanchez et al,[1].

however, the fact that the plume was observed at the Martian terminator makes the *rocket dust storm* mechanism difficult to support.

In the second scenario, it was conjectured the possibility whether the observed plume might be attributable to an aurora, where it is known the existence of strong magnetic field anomalies in the crust at Terra Cimmeria region, and where actually Mars aurora activity have been observed in the past. This hypotheses seems to be in agreement with the meridional extent of the plume above 500 km as well as its variability. However, quantitative estimates of the required aurora intensity defy such a hypotheses and additionally requiring an exceptional influx of energetic particles over days from the Sun, although the solar activity in march 2012 was not unusually high. As was concluded in that research report, both explanations, defy our current understanding of Mars´s upper atmosphere.

In this paper, we will explore a possible mechanism which may rescue the first scenario by providing a source of energy able to lift material from the troposphere well into the thermosphere of Mars but contrary to the *rocket dust storm* mechanism it does not require high insolation but rather high insulation.

1 Formation and collapse of supersaturated tropospheric cavities

1.1 Formation

To begin with, let us consider a certain tropospheric parcel as schematically depicted in Fig. 2-left. This tropospheric parcel is placed just at the top of a dense dust cloud which is -after a local dust storm, gravitationally settling down during the night. The presence of this dense suspended dust cloud between the parcel and the surface translates into an overcooling of the parcel because the dust is impeding the input of heat from the surface and then exacerbating the loss of heat of the parcel.

The magnitude of this overcooling will depend mostly on the optical opacity of the suspended dust below the parcel which can be as large as $\tau = 5$, [4]. In anyway, it is suffice to point out for our descriptive purpose that from the available data registered by Viking landings for several years on the Martian surface, with the arrival of dust storms temperature drops down by 10 to 15 ^{o} K, [5], which referring to Fig. 1, it is within the required overcooling required for condensation of H_2O or CO_2 at the troposphere (< 50 Km).

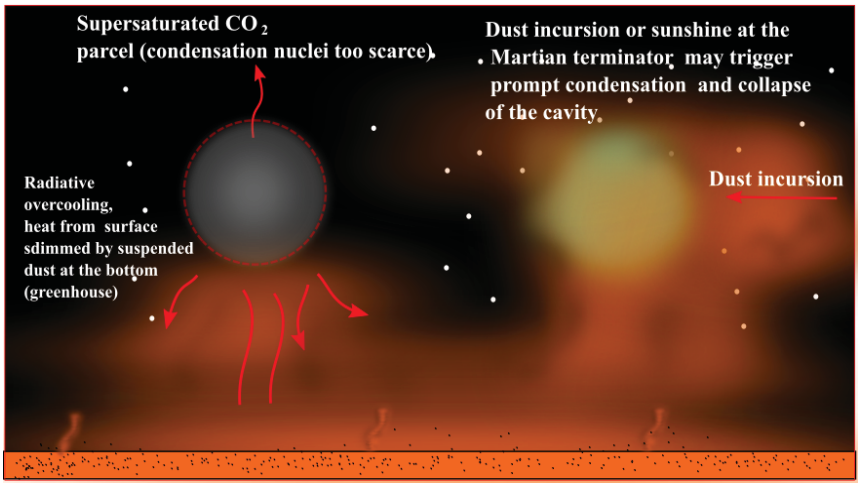

Figure 2: Pictorially sketch of the possible mechanism for the formation of supersaturated tropospheric cavities and collapse on Mars.

Now, if the parcel is devoid of condensation nuclei (dust aerosol on Mars) high supersaturation is possible. This spesaturation has been already observed on Mars from the relatively recent data sent back by the SPICAM spectrometer on board ESA´s Mars Express spacecraft which revealed that the planet´s atmosphere could be supersaturated with water vapor at altitudes of up to 50 km above the surface (troposphere),[6], with extremely high levels of supersaturation -up to 10 times greater than those found on Earth. Once this unstable supersaturated parcel is generated and with the first rays of sunlight in the morning -and the beginning of the daily dust activity, any dust incursion (from the beginning of daily dust activity) might trigger the condensation of the parcel and the formation of a cavity with its subsequent vigorous prompt collapse as schematically depicted in Fig. 2-right.

The proposed mechanism would be analogous to the well know superheated explosions -also known as steam explosions, where a region initially devoid of condensation nuclei explode vigorously if incursion of condensation nuclei occurs disrupting the metastable state. Here is the same, but instead superheating and explosion, we have supersaturation and implosion.

1.2 Collapse and rebound

Immediately after condensation, the cavity will collapse owing to the surrounding pressure. The collapse will continue and the material inside will be progressively compacted as the collapse progresses until at a certain critical density (of the mixture CO_2-ice, H_2O-ice particles and dust) is attained. At this density, the collapse is stopped and the rebound stage starts. An schematic picture of the collapse and rebound stages is given in Fig. 3.

For the sake of analysis and with the purpose to obtain a first estimate of the energy released from such an event, let us assume a spherical cavity small enough in comparison with the surrounding atmosphere and then making allowable the assumption of an infinite mass of homogeneous incompressible atmosphere with pressure and density calculated at the location where the cavity is formed. With this configuration the infalling velocity of the cavity as function of the contraction ratio is given by the generalized Rayleigh equation, [7], as

$$u^2(t) = \frac{2p}{3\rho}\left(\frac{R_o^3}{R^3(t)} - 1\right) \qquad (1)$$

where u is the infalling velocity of the cavity at time t after collapse starts, p and ρ the surrounding atmospheric pressure and density., respectively. R the radius of the boundary cavity at time t, and R_o the ini-

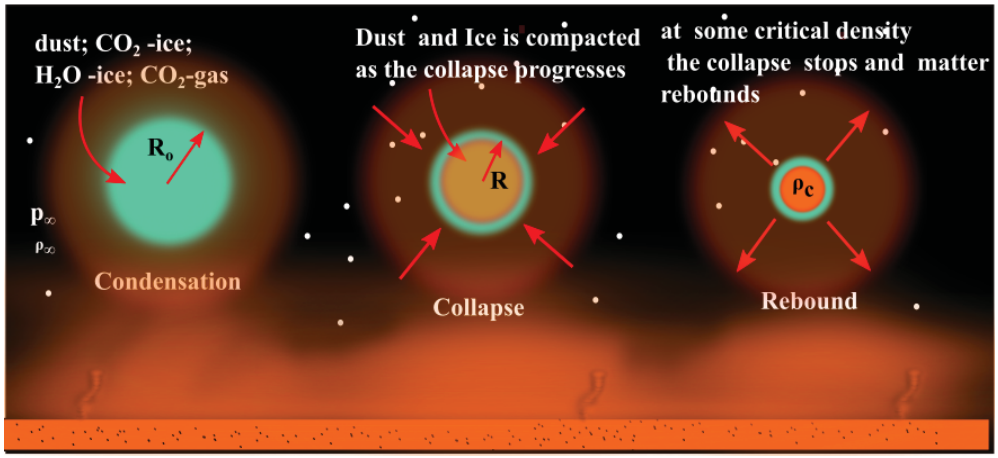

Figure 3: Pictorially sketch of the collapse and rebound phase.

tial value of R, i.e., the initial radius of the cavity at the moment the collapse starts or $t = 0$. On the other hand the whole kinetic energy at time t of the motion is given by

$$E_k = \frac{4\pi}{3} p \left(R_o^3 - R^3(t)\right) \tag{2}$$

As the collapse progresses, the material inside the cavity (mixture CO_2-ice, H_2O-ice particles and dust) attain a certain critical density at which the collapse is stopped followed by a rebound phase. If the critical radius at which the critical density ρ_c is attained is called as R_c, then from Eq.(2) the maximum energy available is

$$E_k = \frac{4\pi}{3} p \left(R_o^3 - R_c^3\right) \tag{3}$$

where by balance of mass inside the cavity we have

$$\frac{R_o}{R} \approx \left[\frac{\rho_c}{\rho}\right]^{\frac{1}{3}} \tag{4}$$

If we assume that the critical density ρ_c is the maximum density of a compacted solid-ice core, then with $\rho_c \approx 10^3$ kg m^{-3} and the density of troposphere on $\rho \approx 10^{-3}$ kg m^{-3}, then $\frac{R_o}{R} \approx 100$.

In order to know how fast the surrounding material will be accelerated when the inside material is rebound, we could use the Gurney equations by analogy with material ejected by explosive detonations surrounding initially the explosive. This equation determines how fast fragments surrounding explosives are released into the surrounding and is given by the generalized expression [8]

$$v^2 = u^2 \left[\frac{M}{C} + \frac{3}{5}\right]^{-1} \tag{5}$$

where v is the velocity of accelerated material surrounding the cavity after implosion-rebound; C is the mass contained in the cavity; M the mass of the accelerated sheet of material.

Inserting Eq.(1) into Eq.(5) one obtains

$$v^2 = \frac{2p}{3\rho}\left[\frac{R_o^3}{R^3} - 1\right]\left[\frac{M}{C} + \frac{3}{5}\right]^{-1} \tag{6}$$

In order to obtain some rough idea or upper limit of the maximum altitude H_{max} attainable by the accelerated material, we can equal the kinetic energy with the potential energy yielding

$$H_{max} < \frac{v^2}{2g} \tag{7}$$

where g is the gravity acceleration which in view of several uncertainties we will take as the surface gravity. By inserting Eq.(6) into Eq.(7), we obtain

$$H_{max} < \frac{p}{3g\rho}\left[\frac{R_o^3}{R^3} - 1\right]\left[\frac{M}{C} + \frac{3}{5}\right]^{-1} \tag{8}$$

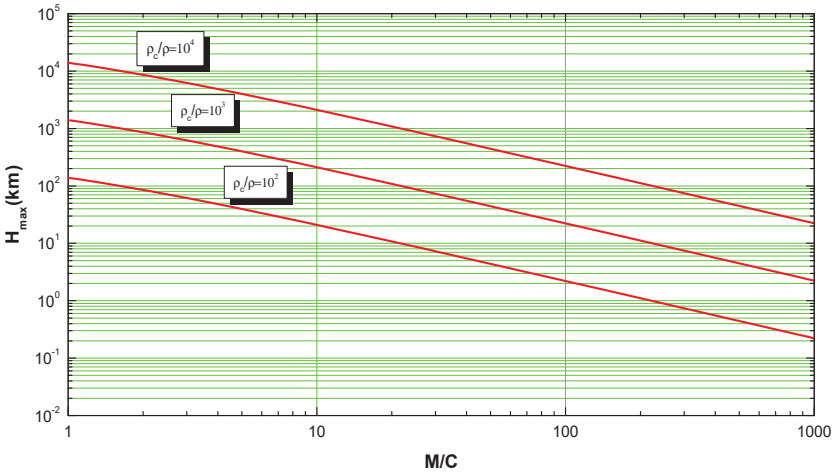

Figure 4: The maximum altitude upper limit as a function of the contraction ratio from Eq.(10).

and taking into account Eq.(4) we get

$$H_{max} < \frac{p}{3g\rho}\left[\frac{\rho_c}{\rho} - 1\right]\left[\frac{M}{C} + \frac{3}{5}\right]^{-1} \qquad (9)$$

Eq.(9) may be simplified further by considering the relation of ideal gases $\frac{p}{\rho} = \frac{\bar{R}T}{\bar{m}}$ where T is the temperature,$\bar{R}$ the gas constant and $\bar{m}$ the molecular mass of the atmosphere. Thus we obtain

$$H_{max} < \frac{\bar{R}T}{3g\bar{m}}\left[\frac{\rho_c}{\rho} - 1\right]\left[\frac{M}{C} + \frac{3}{5}\right]^{-1} \qquad (10)$$

• Discussion

To obtain some idea of the shape of the curves predicted by Eq.(10), we assume some typical values of the parameters: $T = 130$ K; $\bar{m} = 43 \times 10^{-3}$ kg/mol; $g = 3.7$ m s^{-2}. The resulting curves are shown in Fig. 4. It is seen, that with a maximum theoretical value of $\frac{\rho_c}{\rho} =< 10^5$ (if it is is assumed as critical density the density of a solid ice core), there is enough energy to lift material well into thermosphere and even ionosphere. For example, with $\frac{\rho_c}{\rho} < 10^4$ the implosion will be able to lift 100 times the mass of the condensate cavity up to a height of 100 km or thereabouts. Although admittedly this is an idealized calculation where in reality with such high velocities and pressures there would be thermal effects -which had been neglected in the calculation, and also the assumed atmospheric incompressibility is not longer appropriated, nonetheless, it is shown that the conjectured mechanism is potentially able to lift material at high altitudes.

2 The possible role of the magnetic field: *magnetocavities*

At it was mentioned in introduction, it is known the existence of strong magnetic field anomalies in the crust at Terra Cimmeria region, which is given place to the aurora hypothesis for explanation of the March 2012 event.

It is interesting to investigate if the magnetic field at Cimmeria region could play some role within the framework of our proposed mechanism., i.e, in the formation of supersaturated tropospheric cavities. Although cavities could be formed in a number of different ways which can lead to the basic condition, i.e., supersaturation by overcooling, however it could be true that if it is demonstrated that magnetic fields can play some role in the formation of such cavities this will be more completeness to the proposed hypothesis, and in fact, will be possibly the only hypothesis which can merge all the accounts known on the March 2012-event. Fig. 5 shows an illustrative sketch of what we are seeking to investigate in this section. In this picture, we want to know if it is possible that in someway the local magnetic could

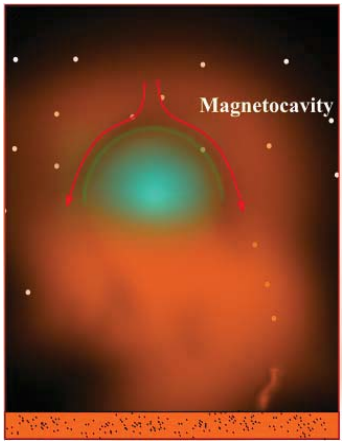

Figure 5: Possible formation of supersaturated cavity induced by the local magnetic field at Cimmeria region.

manage a certain place devoid of dust (allowing high supersaturation).

First of all, it is required that dust particles are electrically charged and then permitting it to respond to the imposed local magnetic field.
It is known that bipolar charging of dust particles (by tribocharging or friction charging process) are generated from dust atmospheric activity on Mars, [9]; [10]; [11]-[13]., and it had been hypothesized that the smaller, or finer, particles tribocharge oppositely to the larger size particles, [14]; [15]; [16];[17] and additionally the particle-size dependence of the charge polarity of particles of dust has been experimentally demonstrated [18].

Now, assuming a bipolar charged dust particles, we need to know if the magnetic energy density (at that region) must be comparable to the kinetic energy density of the charged particles of dust, or putting another way, that the dynamic ram pressure from the dust particles be equal to the magnetic pressure from the Mars's local magnetic field. Taking into account that the low-pressure Martian troposphere gives it a high electrical conductivity -the high electrical conductivity of the atmosphere of Mars could result in an atmospheric electric circuit as proposed by some researchers [19], then the magnetic pressure p_m is given by

$$p_m = \frac{B^2}{\mu_o} \tag{11}$$

and then condition for affecting significatively dust particles yields

$$\left(\frac{\rho_d u_t^2}{2}\right)_d \leq \left(\frac{B^2}{\mu_o}\right) \tag{12}$$

where ρ_d is the charged dust density, u_t the dust settling or terminal velocity, B the magnetic strength at that region and μ_o the vacuum permeability.

If its is assumed spherical dust particles, then the settling velocity is approximately given by

$$u_t^2 = \frac{2\rho_p r_p g}{3\rho_\infty C_d} \tag{13}$$

where ρ_p and r_p are the density and the radius of the particle, respectively., ρ_∞ the atmospheric density through which the particles is falling, C_d is the drag coefficient., and g the acceleration due to gravity. Since the gravitational field varies with distance as $\frac{1}{a^2}$ where a is the radial distance to the center of the planet. Then Eq.(13) becomes.

$$u_t^2 = \frac{2\rho_p r_p g_o a_o^2}{3\rho_\infty C_d a^2} \tag{14}$$

Where g_o is the gravitational acceleration at the surface and a_o the radius of the planet. Finally, the density of the dust is given by

$$\rho_d \approx \frac{4\pi r_p^3 \rho_p N_p}{3} \tag{15}$$

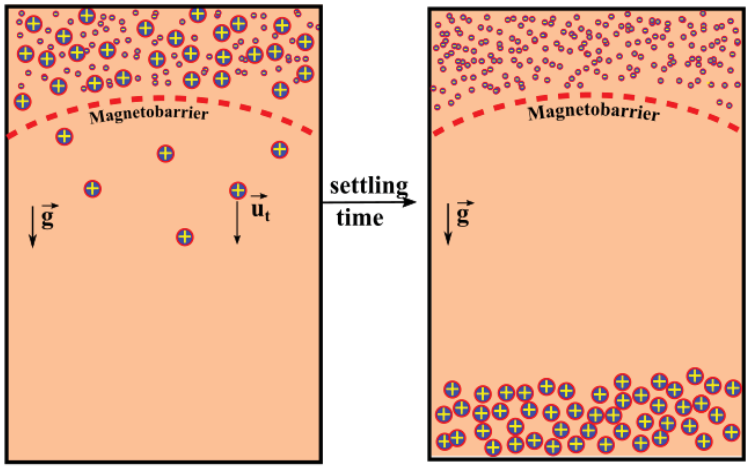

Figure 6: *Magnetobarrier* induced y local magnetic field anomalies acting on charged dust particles on Mars could generate an effective spatial separative mechanism and the formation of cavities or the creation of large local electrostatic fields.

where N_p is the concentration of dust particles per unit of volume. This concentration is as first approximation given as function of the the optical opacity as, [4]

$$N_p = N_o \tau \exp^{-\frac{z}{H}} \tag{16}$$

where $N_o = 6 \times 10^6$ m^{-3} is the number density at the surface when the optical depth $\tau = 1.$, and $H = 10$ km is the atmospheric scale height for Mars. Substituting terms, Eq.(12) becomes

$$B > \frac{2\rho_p a_o r_p^2}{3a} \left[\frac{\pi N_o \tau \exp^{-\frac{z}{H}} g_o \mu_o}{\rho_\infty C_d} \right]^{\frac{1}{2}} \tag{17}$$

According with Eq.(17) there would be some induced *magnetobarrier* for small particles as is schematically depicted in Fig. 6.

• Discussion

Assuming some reasonable values of the parameters: $\rho_p \approx 3 \times 10^3$ kg m^{-3}, [4]; dust suspended at a tropospheric distance of 10 km; and then $\frac{a_o}{a} \approx 0.98$; $N_o = 6 \times 10^6$ m^{-3}; $z = 10$ km and scale height $H = 10$ km, [4]; $g_o = 3.7$ m s^{-2}; $\rho_\infty = 10^{-2}$ kg m^{-3}; and $C_d \sim 0.5$, then we get

$$B > 157 \times \tau^{\frac{1}{2}} r_p^2 \tag{18}$$

with B in (nT); and r_p in (μm).

The resulting curves are shown in Fig. 7. It is seen, that magnetic anomalies on Mars will be able to separate dust particles of a few micrometers from large particles. This mechanism could enhance the formation of cavities devoid of dust. Also it is interesting to see, that the smaller particles will be on the top of the cavity, which means that at the moment of the collapse of the cavity and rebound, small particles will be preferentially propelled to high altitudes. This fact seems consistent with the best fit obtained for the effective radii of particles CO_2-ice particles of 0.1μm for the March 2012 event, [1].

NOMENCLATURE

a = distance from center of planet to center of cavity
a_o = radius of the planet
B = magnetic field
C = mass contained in the cavity
C_d = drag coefficient
E_k = kinetic energy
g_o = gravity at surface
g = gravity
H = length scale
H_{max} = maximum permissible altitude
M = mass of the accelerated sheet of material

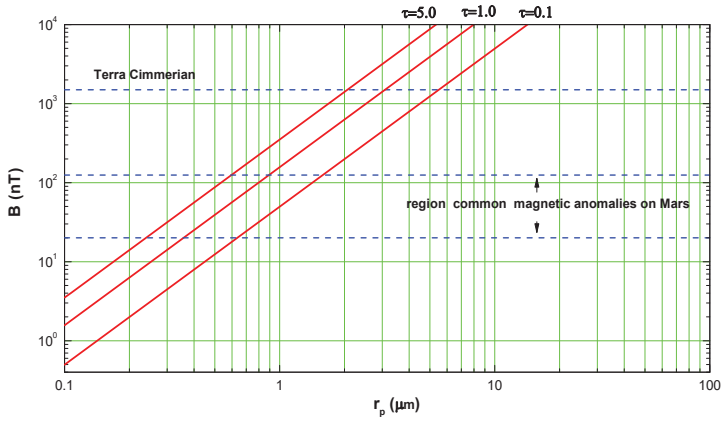

Figure 7: Predicted curves by Eq.(18) for several values of dust storms.

$\bar{m}$ = mean molecular mass of atmosphere
N_p = number density of particles per unit volume
p = pressure
r_p = radius of particles
R = actual radius of cavity
$\bar{R}$ = gas constant
R_o = initial radius of cavity
R_c = critical radius of cavity
u = infalling radial velocity of collapsing cavity
u_t = terminal velocity of particles
v = velocity ejected material surrounding the cavity
t = time
T = temperature
z = vertical distance

Greek symbols
ρ = density
ρ_c = critical density
ρ_d = density of dust cloud
ρ_p = density of particles
ρ_∞ = density of atmosphere
τ = optical opacity
μ_o = magnetic permeability of vacuum

subscripts
d = dust; drag
o = reference, surface
p = particle
e = Earth
m = Mars

Acknowledgements

This research was supported by the Spanish Ministry of Economy and Competitiveness under fellowship grant Ramon y Cajal: RYC-2013-13459.

References

[1] Sanchez-Lavega A., Munos G.A., et.al. 2015. An Extremely high-altitud plume seen at Mars´Morning Terminator. Nature Letter, 518. 525-527.

[2] Gonzales-Galindo F., Maatttanen A., Forget F., Spiga A. 2011. The Martian Messosphere as revelaed by CO_2 cloud observations and general circulation modelling. Icarus. 216. 10-22.

[3] Spiga A. et.al. 2012. Rocket dust storms and detached dust layers in the Martian atmosphere, Journal Of Geophysical Research: Planets, Vol. 118, 746.

[4] Haberle R.M., Mckay C.P., Pollack J.B. et.al. 1993. Atmospheric effects on the Utility of Solar Power in Mars. Resources of Near Earth Space, pp. 799-818.

[5] Ehrlich P.R., Sagan C., Kennedy D. The Cold and the Dark: The World After Nuclear War. Norton, 1985.

[6] Maltagliati L., Montmessin F., Fedorova A., Korablev O., Forget F., BertauxJ.L. 2011. Evidence of Water Vapor in Excess of Saturation in the Atmosphere of Mars. 333, 6051, pp. 1868-1871

[7] Rayleigh Lord. 1917. On the pressure developed in a liquid during the Colllapse of a Spherical cavity. Phil. Mag, 34, 94-98

[8] Cooper Paul W. 1996. Acceleration, Formation, and Flight of Fragments. Explosives Engineering. Wiley-VCH. pp. 385-394. ISBN 0-471-18636-8.

[9] Eden, H. F., and B. Vonnegut. 1973. Electric breakdown caused by dust motion in low-pressure atmospheres: Considerations of Mars, Science, 180, 962-963.

[10] Mills A. A. 1997. Dust clouds and frictional generation of glow discharges on Mars,Nature, 268, 614

[11] Erika L. Barth, William M. Farrell, Scot C.R. Rafkin. 2016. E< Icarus. 268, 253-265

[12] Ping Wang., Xiaojing Zheng. 2015. Unsteady saltation on Mars. Icarus, 260, 161-166

[13] Farrell W.M., McLain J.L., Collier M.R., Keller J.W., Delor J.T. 2015. Is the electron avalanche process in a martian dust devil self-quenching?. Icarus, 254, 333-337

[14] Freier G. D. (1960), The electric field of a large dust devil, J. Geophys.Res. 65, 3504.

[15] Crozier W. D. 1964. The electric field of a New Mexico dust devil, J. Geophys. Res.69, 5427-5429.

[16] Stow C. D. (1969), Dust and storm electrification, Weather, 24, 134-139.

[17] Renno N. O., and J. F. Kok. 2008. Electrical activity and dust lifting on Earth, Mars and beyond, Space Sci. Rev. 137, 419-434

[18] Forward K. M., Lacks D.J., Sankaran R.M. 2009. Particle-size dependent bipolar charging of Martian regolith simulant. Geophys. Res., 36, 1-5

[19] Farrell, W. M., and M. D. Desch (2001), Is there a Martian atmospheric electric circuit, J. Geophys. Res., 106(E4), 7591-7595.

EPSC Abstracts
Vol. 11, EPSC2017-152, 2017
European Planetary Science Congress 2017

Can We Detect Changes in the Solar Flattening with an Artificial Planet?

David E. Smith and Maria T. Zuber
Department of Earth, Atmospheric and Planetary Sciences, Massachusetts Institute of Technology, Cambridge, MA 02139-4307, USA. (smithde@mit.edu)

Abstract

The gravitational quadrupole moment of the sun provides information on internal structure and dynamics. Estimates of this parameter from helioseismology are uncertain and model dependent. A proposed approach to improve estimation by tracking Mercury and an artificial planet, out of the plane of the ecliptic, is discussed.

1. Introduction

The sun is a gaseous body with a dynamic interior that likely has a gravity field that changes with time due to processes that cause 11- and 22-year cycles in solar electromagnetic output, particle radiation, and changes in the solar magnetic field. The magnitudes of these changes, if they exist, are speculative, but dynamic models and helioseismological results suggest a gravitational flattening of degree 2 [e.g., 1-6] exists, although there is no evidence for temporal variations.

To estimate the gravity field of a planet, tracking data of one or more spacecraft are generally analyzed for their gravitational perturbations. The present dynamic solutions for the degree-2 solar gravity field are derived from the orbital motion of Mercury, which has an orbit of near-zero inclination (~4^o) with respect to the solar equator, thus limiting its accuracy and the ability to detect any variation. We suggest that improvements and possible changes in the present degree-2 zonal coefficient in the solar gravity field, could be obtained if an additional "planet" in a similar orbit to Mercury existed, but at a higher orbital inclination.

2. An Artificial Planet

We suggest that an artificial planet, referred to here as AP1, could be placed in an orbit inclined to the ecliptic and tracked by optical or microwave systems to provide the orbital behavior of AP1 at the highest possible accuracy for a period of several years [cf. 7]. In combination with orbital data already available for Mercury from the MESSENGER mission, and data expected from the upcoming BepiColombo mission, estimates of the degree- and order-2 solar gravity field, and its possible variation, could be obtained, or at least bounded. Figure 1 shows a sketch of the general concept.

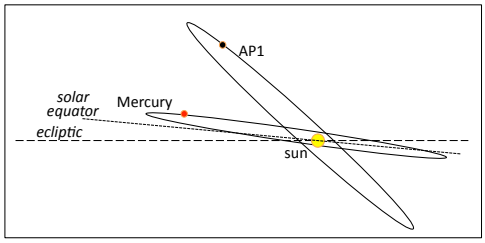

Figure 1: Concept of Mercury and an artificial planet (AP1) for estimating the low-degree solar gravity field.

3. Orbit

The orbit of AP1 will need to be a balance between the desire for a substantially higher inclination than Mercury and the ability to achieve the out-of-the-ecliptic trajectory necessary at launch. As the inclination increases, the sensitivity to the zonal coefficients of degree 2 becomes less. For the orbit of Mercury and the proposed orbit of AP1, the ability to detect any degree-3 or higher gravity terms are almost impossible due to the radii of the orbits being approximately 100 times the solar radius. We suggest an orbital radius similar to that of Mercury would be adequate because we know that at that distance the degree-2 zonal term is measureable. But a closer orbit would be much preferable, if physically possible, and would improve the chances of detecting any variations, both zonal and longitudinal.

Attaining a high solar inclination is challenging but has been achieved in the past, as for example the Ulysses mission, which used a gravitational assist from Jupiter to obtain a solar inclination of ~79^o [8].

The detection of the solar gravity field will most likely be from the secular or long-period perturbations of the node and argument of perihelion, and so it is advisable to avoid an inclination of ~63.4^o where the degree-2 motion of the perihelion is zero. In addition, if there is any possibility of detecting the degree-3 zonal term, then an inclination of ~31.1^o should be avoided. We therefore suggest an inclination to the solar equator of 45^o to 50^o would ensure an observable signal from the degree-2 gravity field from the motion of both the node and perihelion.

4. Radiation & Tracking

Equally challenging will be the compensation of solar radiation pressure, nearly 7 times larger at Mercury than at Earth, and thus likely requiring some form of "drag-free" system. However, systems on Earth-orbiting spacecraft have managed to compensate for air drag, a much larger force than that from solar radiation at Mercury. The tracking of the AP1 could be performed at microwave or optical frequencies, but the former will require a large antenna that might make the s/c more massive and complicated than we think necessary. We therefore believe laser tracking is preferable.

5. Summary and Conclusions

An artificial planet in an appropriate orbit will be sensitive to the degree-2 gravity field of the sun. Observation of Mercury's orbit from observations of the MESSENGER spacecraft have already estimated the degree-2 zonal term, but there is a probability that the coefficient could be changing slowly as result of decadal periodic changes occurring within the sun. Observations of the orbital motion of another planetary body in a similar orbit to Mercury, together with present and future Mercury observations, would improve the accuracy and may enable any long period changes to be detected. Such a detection would provide evidence of present-day structural and dynamic processes deep within the sun, possibly related to the 11- and 22-year solar cycle.

We recognize that the design and operation of this mission will not be trivial, but if we can measure the changes in solar gravity field, and infer changes occurring deep in the solar interior, we will have advanced our understanding of our solar system and of the dynamics of sun-like stars.

References

[1] Goldreich, P. and Schubert, G.: A theoretical upper limit of the solar oblateness, Astrophys. Jour., 154, 1005-1010, 1968.

[2] Gough, D.O.: Internal rotation and the gravitational quadrupole moment of the Sun, Nature, 298, 334-229, 1982.

[3] Mecheri, R. et al.: New values of gravitational moments J2 and J4 deduced from helioseismology, Solar Phys., 222, doi: 10.1023/B:SOLA.0000043563.96766.21, 2004.

[4] Pitjeva, E.V.: Relativistic effects and solar oblateness from radar observations of planets and spacecraft, Astron. Lett., 31, 378-387, 2005.

[5] Pijpers, F.P.: Helioseismic determination of the solar gravitational quadrupole moment, Mon. Not. R. Astron. Soc., 297, L76-L80, 1998.

[6] Williams, J.G. et al.: DE430 Lunar Orbit, Physical Librations, and Surface Coordinates, Jet Propulsion Laboratory Interoffice Memorandum IOM 335-JW, DB, WF-20130722-016, July 22, 2013.

[7] Shapiro, I.I. et al.: Mercury's perihelion advance: Determination by Radar, Phys. Rev. Lett., 28, doi: https://doi.org/10.1103/PhysRevLett.28.1594, 1972.

[8] Marsden, R.G. et al.: Ulysses at high heliographic latitudes: An introduction, Astron. Astrophys., 316, 279-286, 1996.

EPSC Abstracts
Vol. 11, EPSC2017-205, 2017
European Planetary Science Congress 2017

Earth variable rotation and climate oscillations

L. Zotov (1,2), N. Sidorenkov (3) and C. Bizouard (4)
(1) National Research University Higher School of Economics, Moscow Institute of Electronics and Mathematics, Moscow, Russian Federation (wolftempus@gmail.com) (2) Sternberg Astronomical Institute, Lomonosov Moscow State University (3) Hydrometeocenter of Russia, Moscow (4) SYRTE, Service de la Rotation de la Terre, Observatoire de Paris, PSL Research University, CNRS, Sorbonne Universites, UPMC Univ. Paris 06, France

Abstract

Our epoch of precise observations of Earth systems is already giving us an evidence of interconnection between climate processes and Earth rotation changes. Amplitude of the Chandler wobble decreased sufficiently in the 2010s, as in the 1930s. 70-year modulation is observed in the Length of Day (LOD) changes. At the same time Earth temperature and sea level variations, well observed after removal of the global warming trend, have similar periodicity. The temperature extrema, usualy related to the Multidecadal Atlantic Oscillatons are observed in the 1930th and 2000 and, coinciding with the extrema of LOD. We analyze Chandler wobble phase and amplitude changes, its excitation sources, trying to bridge this traditional subject of geodesy with contemporary climatological observations over ocean, atmosphere, and land mass transport.

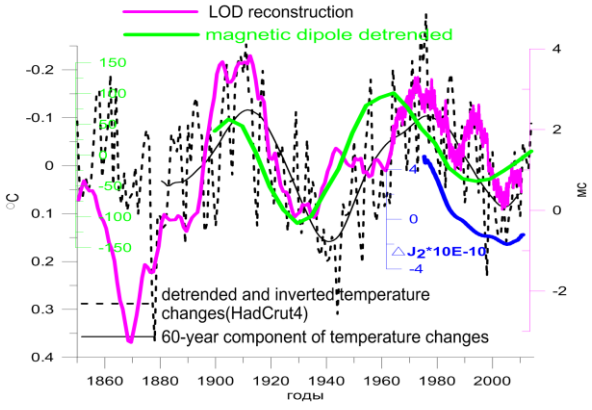

Fig. 1 Length of day changes, 60-year temperature changes (inverted), trend in the Earth gravity J_2 coefficient, and magnetic dipole strength detrended.

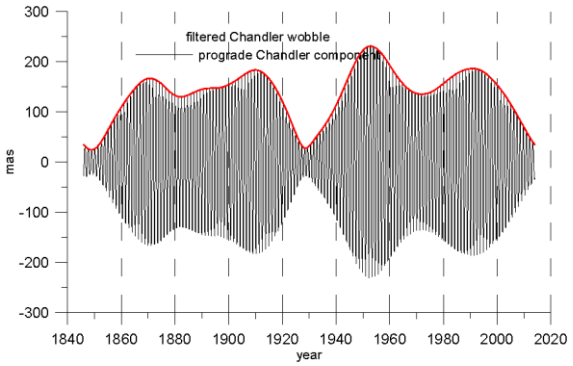

Fig. 2 Chandler wobble of the Earth pole (X-component) and its envelope.

Acknowledgements

We thank Paris observatory for one month-position, and Higher School of Economics for support.

References

[1] Lyubushin A.A. Geophysical Monitoring Data Analysis (RUS), Moscow, Nauka, 2007 http://alexeylyubushin.narod.ru/Geophysical_Monitoring_Systems_Data_Analysis_Book_Rus.pdf

[2] Zotov L., Bizouard C., Shum C.K. A possible interrelation between Earth rotation and climatic variability at decadal time-scale , Geodesy and Geodynamics, Volume 7, Issue 3, May 2016, Pages 216-222, KeAi, China, doi:10.1016/j.geog.2016.05.005, 2016.

EPSC Abstracts
Vol. 11, EPSC2017-426, 2017
European Planetary Science Congress 2017

Simulating hyperspectral images for Martian 3D scenes.

S. Douté IPAG, Université Grenoble Alpes, Bât OSUG A CS 40700 38058 Grenoble Cedex 9 France
(sylvain.doute@univ-grenoble-alpes.fr)

Abstract We present a tool for simulating hyperspectral images for 3D Martian scenes. Several lines of development are considered for achieving a high degree of realism : high resolution digital elevation models, description of material distribution with fractal characteristics, bidirectional reflectance measured in the laboratory as a function of geometry and wavelength for a series analogue materials, mixing of spectral signatures at different scales, 3D radiative transfer between atmosphere and surface. The simulator addresses two main needs (i) developing and testing methods for the correction of atmospheric and photometric effects images taken by orbiter around Mars (ii) developing and testing methods for the linear and nonlinear spectral unmixing applied to hyperspectral images.

Methods A synthetic hyperspectral image is generated according to a given scene, atmospheric conditions, « sensor » characteristics, and observation geometry. For that purpose several modules are implemented that reflect different steps in the simulation.

Description of the material distribution and abundances. The spatial distribution of materials covering the scene is described by maps of pure component - a.k.a "endmembers" - abundances. The latter are generated by a genetic algorithm - a cellular automaton - reproducing some planetary transport and mixing processes for achieving fractal properties as expected for real scenes in nature. The cellular automaton consists on an iterative process starting with seeds of pure materials distributed within the scene and performing actions between pixels such as mixing and gradient controlled diffusion. The user can define roughly the distribution of the endmembers by defining the seeds, the different probabilities for each action, the size of the neighborhood window, and the total number of iterations. For instance, if the probability of mixing is high the resulting abundance maps will be very mixed.

Spectro-photometric properties of the materials in the scene. In the simulation, the bidirectional reflectance of the surface materials is expressed either using the Hapke model or the Ross-Thick Li-Sparse (RTLS) model: $\rho(\mu_0,\mu,\varphi) = k^L + k^G f_G(\mu_0,\mu,\varphi) + k^V f_V(\mu_0,\mu,\varphi)$ The subscripts refer to Lambertian (L), geometric (G) and volumetric (V) components with f_G and f_V predefined geometric kernels. This model has proved to be accurate in recreating many types of natural surfaces [1]. Several modalities of the RTLS model were extracted by our tool MARS-ReCO [2] for varied Martian geological contexts from the processing of multi-angular hyperspectral observations by the Compact Reconnaissance Imaging Spectrometer for Mars (CRISM). On the other hand the bidirectional reflectance of eight natural well-controlled samples of planetary interest was measured as a function of wavelength in the visible and infrared for a large range of phase angles [10-130°] with a spectrophoto-goniometer [3].

Modeling of mixtures. The components can coexist at two main subpixel levels: macroscopic (linear spatial mixing) and/or microscopic (non linear granular mixture). In the case of a purely linear mixture, the endmember abundances are areal fractions $a_r, r = 1, ..., R$ (nb of endmembers). In the case of a purely intimate mixture, the endmember abundances are fraction number of grains $f_r = 1, ..., R$ (nb of endmembers). In the case of a mixtures of mixtures, the endmember abundances are built from areal fractions $a_r, r = 1, ..., R+1$ and fraction number of grains $f_r = 1, ..., R$ so that the abundance of endmember r is $a_r + a_{R+1} * f_r$. The Hapke parameters (w, b, c, θ) of an intimate mixture are obtained from the photometric parameters of each pure compound $(w_r, b_r, c_r, \theta_r)$ and from the abundance maps according to the mixing rules proposed by [4] derived from MonteCarlo ray-tracing experiments that we parametrized.

Computation of the geometrical and illumination conditions. The scene is also defined by a high-resolution (10m.pixel-1) high quality Digital Elevation Model (DEM) that we generate from the fusion of photogrammetry and photoclinometry information derived from CTX@MRO imagery [5]. Then maps of local geometrical and illumination conditions can be calculated considering the sun elevation θ_S and northern azimuth ϕ_S as well as the viewing zenith angle VZA and the phase angle g as a function of the

pixel geographical coordinates. The atmospheric condition is defined by the aerosol radiative properties, their vertical distribution and an integrated Aerosol Optical Depth (AOD). At this point the atmospheric radiative LUT of MARS-ReCO [2] provides the direct and diffuse wavelength dependent illumination for a flat ground. We use an improved version of the parametrization by [6] for adapting these fluxes to any slope characterized by its magnitude and orientation. In addition one needs to consider the fraction of sky visible and to care about possible shadowing and occultation of a given facet by neighboring topography. Highly efficient discrete geometrical calculations implemented on GPU are performed on the DEM for that purpose.

Surface-atmosphere radiative transfer calculations for computing the image. The calculation of the spectral radiance at the sensor is based on (i) the Hapke or RTLS model fed by the macroscopic spectrophotometric parameters for computing the reflectance of the surface and (ii) a 3D surface-atmosphere radiative transfer (RT) scheme inspired by [7] and addressing environmental effects (i.e. reflections of direct and diffuse irradiance from the neighborhood) and the multiple scattering between the surface and the atmosphere. The upward transfer of the surface reflected radiance to the sensor either by direct path or by multiple scattering is implemented with a 1D RT scheme.

Results Series of synthetic images are produced to validate the direct simulation code and to perform a sensitivity analysis of the model regarding its different parameters. In particular we can compare qualitatively and quantitatively real imagery with twin synthetic images produced by our tool according to the same atmospheric and geometric conditions using spectrophotometric properties extracted from CRISM observations by our tool MARS-ReCO (Fig. 1).

Acknowledgements This research was carried out under the project " I2- Mars" conjointly funded by the Agence Nationale de la Recherche (ANR) (grant number ANR-12-IS05-0001-01) and the National Science Foundation of China (NSFC).

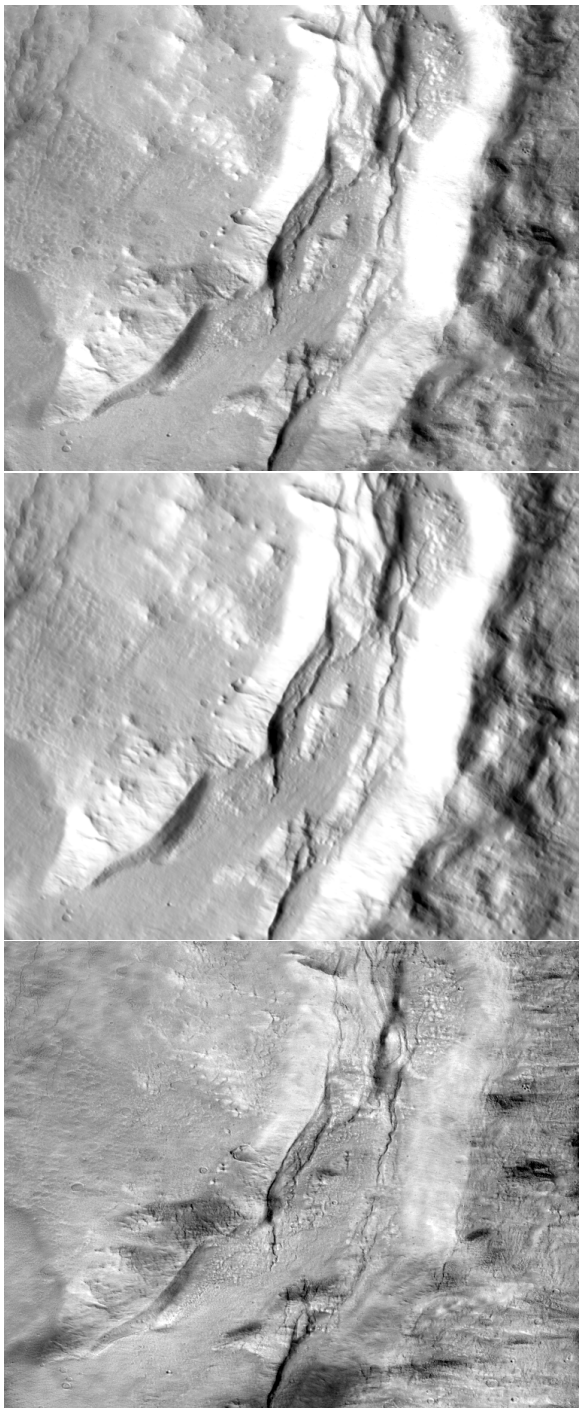

Figure 1: Comparison for a region of interest between an original CTX image (top) and a synthetic counterpart image produced by our tool (middle). For the latter the surface is considered to be homogeneously covered by a single material owning the average spectro-photometric properties of the region as extracted from a CRISM observation by our tool MARS-ReCO. We also show the ratio of the two former images revealing albedo variations intrinsic to the surface independently to the illumination conditions (bottom)

References

[1] W. Lucht et al. *TGRS*, 38(2):977–998, 2000.
[2] Ceamanos X. et al. *JGR planets*, 118:1–20, 2013.
[3] C. Pilorget et al. *Icarus*, 267:296 – 314, 2016.
[4] C. Pilorget et al. *Icarus*, 250(0):188 – 203, 2015.
[5] C. Jiang and Douté S. *ISPRS*, in revision:2017.
[6] A. Spiga and F. Forget. *GRL*, 35:15201–+, 2008.
[7] Mieschet al. *Applied Optics*, 39:6830–6846, 2000.

EPSC Abstracts
Vol. 11, EPSC2017-433, 2017
European Planetary Science Congress 2017

Statistical analysis of the Martian topography

F. Landais(1), F. Schmidt (1), S. Lovejoy (2)

(1) Univ Paris-Sud/CNRS, GEOPS, UMR8148, Orsay, F-91405, France, (francois.landais@u-psud.fr)(2) Physics, McGill University, Montreal, Quebec

Abstract

We investigate the scaling properties of the topography of Mars. Planetary topographic fields are well known to exhibit (mono)fractal behaviour. Still, a single fractal dimension is not enough to explain the huge variability and intermittency. Previous studies have shown that fractal dimensions might be different from a region to another, excluding a general description at the planetary scale. In this project, we are analyzing the Martian topographic data with a multifractal formalism to study the scaling intermittency. In the multifractal paradigm, the local variation of the fractal dimension is interpreted as a statistical property of multifractal fields. The results suggest a multifractal behaviour from planetary scale down to 10 km. From 10 km to 600 m, the topography seems to be simple monofractal. This transition indicates a significant change in the processes governing the Red Planet's surface. Using a comparative planetology approach, we will bring new elements to discuss the place of Mars among the telluric bodies.

.

1. Introduction

The acquisition of altimetric data from Mars Orbiter Laser altimeter (MOLA) has motivated numerous analysis of the Martian topography, in particular the surface roughness. A possible approach is to assume that topography can be mathematically described as a statistical field with quantitative parameters able to characterize the geological units. Many statistical indicators have been proposed and widely explored in order to study the surface of Mars: RMS height, RMS slope, median slope [1], autocorrelation length [2]. Useful information has been obtained by the use of those indicators but they have the disadvantage of been defined at a given scale. By construction, they do not directly take into account the well-established scale symmetry that generally occurs in the case of natural surfaces. Indeed, statistical parameters like the mean or the standard deviation exhibit dependence toward scales. Hence the nature of this dependence needs to be accurately described, otherwise the description of the surface remain incomplete. This subject has been widely studied in the past, parallel to the development of the notion of fractals [3]. More interestingly, the fractal theory provides a mathematical formalism to describe the scale dependence of statistical parameters toward scales. It turns out that simple power-law relations efficiently approach the variability of planetary surfaces. The associated power-law exponent provides a quantitative parameter that is a good scale-independent candidate to characterize the geometric properties of a natural surface. A common example is given by the power spectrum of topographic field providing roughness information in the frequency space as done locally for the Moon [4].

On Mars, different authors have explored the scaling properties of topography by the use of scale invariant parameters. The observed local variation [5] apparently rejects the idea of a global description of any topographic field at the planetary scale. However, modern developments in the fractal theory might be able to give full account to the observed variability and intermittency. As proposed by [6], it is possible to extent the fractal interpretation of topography to a multifractal statistical object requiring an infinite number of fractal dimensions (one for each statistical moment).

2. Data and methods

We used the MOLA instrument database to study Mars [7]. The absolute vertical accuracy is ~10 m but depends on accuracy of reconstruction of radial spacecraft orbit. The surface spot size is 130 m. The along-track point spacing is 330 m. The across-track shot spacing depends on mapping orbit and vary with latitude since the orbit is quasi- polar.

The MOLA topography database is available in the PDS archive. This database has been filtered from noise and atmospheric clouds reflectors. We used the

MOLAUtils tools developed to extract all the points in a given surface [8].

The haar fluctuations [9] are computed for all the available along-track points on the MOLA database and splitted in 74 bins of scale form 600m to the planet scale. For each bin of scales, 21 statistical moments are computed (order 0.1 to 2, step 0.1).

.

3. Results

Figure 1 is the main result of this analysis. Although the linear correlation (scaling) is satisfying, two distinct scaling regimes occur with a transition around 10 km. Figure 2 presents the slope of the linear fit for different moments.

Multiscaling seems to occur on a large but restrict- ed range of scale (superior to 10 km) with a Hurst exponent H = 0.52. At smaller scale, the topography is still scaling but the symmetry is only monofractal with a parameter H = 0.75.

Additionally, we present a similar analysis on different bodies in the solar system (Earth Mars Moon and Mercury) in a comparative way. Interesting similarities arise between Mars on other planetary body.

We demonstrate that a change of processes governing the Martian topography occurs at 10 km [10]. A multiplicative cascade process is occurring at scale higher than 10 km but a simpler monofractal scaling process is occurring a small scale. Craterisation is well known to be a fractal process with a single fractal dimension [4]. We propose that the low scales are dominated by craterisation processes, at the origin of the monofractal scaling law, as suggested [1]. Most probably, other effects, such erosion and volcanism, should be dominant at larger scales.

4. Figures

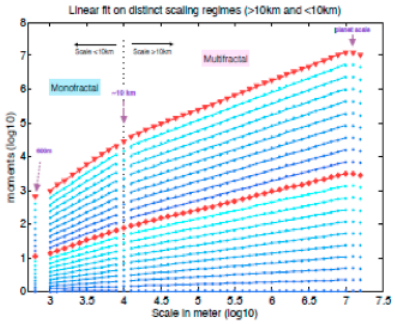

Figure 1: Linear fit on the two different scaling regimes (inferior and superior to 10 km) for every 21 statistical moments from 0.1 to 2.

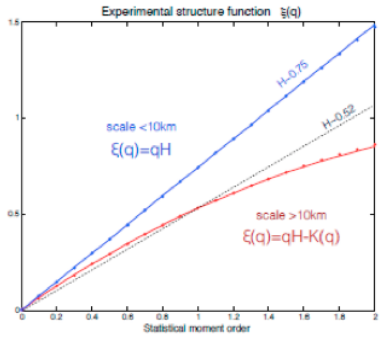

Figure 2: Theoretical structure function ς(q) combining the 21 linear fits shown on figure 1. Red points (resp.blue points) correspond to the range of scales superior (resp. inferior) to 10km

References

References: [1] O. Aharonson, et al. JGR : Planets, 106(E10):23723–23735, 2001. [2] M. A. Kreslavsky and J. W. Head. JGR: Planets, 105(E11):26695–26711, 2000 [3] B. Mandelbrot, Science, 156(3775):636–638, 1967. [4] M. A. Rosenburg, and O. Aharonson. JGR: Planets, 2015. [5] R. Orosei, et al. JGR: Planets , 108, 2003 [6] S. Lovejoy and D. Schertzer, JGR: Atmos- pheres, 95(D3):2021–2034, 1990. [7] D. E. Smith et al, JGR: Planets, 106 (E10):23689–23722, 2001. [8] **http://planeto.geol.upsud.fr/MOLAutils,50.html?lang=en** [9] S. Lovejoy and D. Schertzer. NPG 19(5):513–527, 2012. [10] Landais, F., Schmidt, F. & Lovejoy, S. (2015), Nonlinear Processes in Geophys- ics, 22, 713-722

EPSC Abstracts
Vol. 11, EPSC2017-587, 2017
European Planetary Science Congress 2017

Catching comet's particles in the earth's atmosphere

O. Potashko
Independent researcher , Kiev, Ukraine, (oleksandr.potashko@gmail.com)

Abstract

How to catch cometary particles by using balloons and to make this method steady and reliable. Why are the comet particles interesting? The nature of a comet is full of puzzles; many researchers think that comets may give keys to the origin of the Solar System and origin of life on the Earth.

The project is intended to catch cometary particles in the atmosphere by using balloons. The investigation is based upon knowledge that the Earth crosses the comet's tails during the year. One can catch these particles at different altitudes in the atmosphere. So, we will be able to gradually advance in the ability to launch balloons from low to high altitudes and try to catch particles from different comet tails. The maximum altitude that we have to reach is 40 km. Both methods - distance observation and cometary samples from mission Stardust testify to the presence of organic components in comet's particles. It would be useful to know more details about this organic matter for astrobiology; besides, the factor poses danger to the Earth. Moreover, it is important to prove that it is possible to get fundamental scientific results at low cost.

In the last 5 years launching balloons has become popular and for the movement looks like hackers' one – as most of them occur without launch permission to airspace. The popularity of ballooning is caused by low cost of balloon, GPS unit, video recording unit. Once one uses smartphone, one has a light solution with GPS, video, picture and control function in one unit. The price of balloon itself begins from $50; it depends on maximum altitude, payload weight and material. Many university teams realized balloon launching and reached even stratosphere at an altitude of 33 km. But most of them take only video and picture. Meanwhile, it is possible to carry out scientific experiments by ballooning, for example to collect comet particles.

There is advanced experience at the moment on mineral, chemical and isotopic analysis techniques and data of the comet's dust after successful landing of Stardust capsule with samples in 2006.

Besides, we may use perfect material to catch particles in the atmosphere, which was used by cosmic missions such as Stardust and Japanese Hayabusa. As to balloon launches, we could use Indian Space Research Organization experience that launched a balloon to stratosphere in 2009 and successfully caught particles with organics at an altitude of 42 km.

The main aim of the project is to catch cometary particles by using balloons and to make this method steady and reliable. Why are the comet particles interesting? The nature of a comet is full of puzzles; many researchers think that comets may give keys to the origin of the Solar System and origin of life on the Earth.

EPSC Abstracts
Vol. 11, EPSC2017-624-1, 2017
European Planetary Science Congress 2017

Measuring the Earth's global radiation balance through orbital dynamics

O. Wilkman (1), J. Herranen (2), J. Virtanen (1), J. Näränen (1), J. Peltoniemi (1), M. Gritsevich (2), S. Lahtinen (1), H. Koivula (1), A. Penttilä (2), M. Poutanen (1), K. Muinonen (2,1)
(1) Finnish Geospatial Research Institute, Masala, Finland (olli.wilkman@nls.fi),
(2) Department of Physics, University of Helsinki, Finland

Abstract

We study the possibility of estimating the global scattered radiation flux of the Earth by its radiation-pressure effect on satellite orbits. We perform numerical simulations of typical GNSS orbits, computing various estimates of the magnitude of this effect. We find that changes to orbits caused by reasonable changes in Earth albedo are within detectable limits of modern observational technology, as long as other perturbing forces are modeled well enough.

1 Introduction

We are studying the retrieval of the spherical albedo and net scattered (short-wave) radiation of the Earth from the perturbations caused by the planet's radiation on the dynamics of its satellites. The spherical or Bond albedo gives the ratio of the fluxes incident on and scattered by the planet. The net radiation represents the net heat input into the planet's climate system and drives changes in its atmospheric, surface, and ocean temperatures.

The spherical albedo is the average of the surface albedo of the Earth, which varies greatly depending on the terrain. The polar ice caps have albedos as high as 0.7 while forests and the sea are darker. The global albedo of the Earth is approximately 0.31.

The radiation flux from the Earth illuminates orbiting satellites, which causes a radiation-pressure force. The direction and magnitude of this force depends on the satellite's position in orbit, but generally it causes a radial pressure away from the Earth of some nano-Pascals. For a typical GNSS satellite cross section, this is an acceleration in the order of 10^{-10} m/s^2 [1, 2]. A related radiation-pressure force is caused by the thermal (long-wave) radiation, from emission of absorbed Solar energy, which must be modeled similarly, but has a different distribution on the Earth's surface.

Satellite laser ranging (SLR) is a method of measuring distances to satellites using precise timing of laser pulses. Many satellites, such as the Russian GLONASS and European Galileo GNSS satellites, are equipped with laser retroreflectors, which allow laser ranging to high altitude orbits. Ranges to satellites from a ground station can be measured with an accuracy of centimetres, depending on the satellite altitude and SLR system specifications.

The ultimate aim of the study is inverting the problem and estimating the Earth albedo based on observations of satellites. Observing the orbital positions of a constellation of satellites surrounding the Earth, like GLONASS and Galileo, could provide simultaneous global information on the radiation flux of the Earth.

Modeling these forces truly accurately requires a detailed treatment of the spacecraft shape and reflection properties. Advancement of these techniques is one of the sub-goals of this project.

2 Methods

Here we investigate the effect of the spherical albedo on satellite orbits with the help of a simplified model. We simulate the propagation of satellite orbits using a new orbital simulation software. The simulation can be configured to take into account any combination of the main perturbing forces on medium and high Earth orbits [3].

The orbits studied were Galileo-like, with 56° inclination and a 14-hour period. The orientation of the satellite is derived from the yaw-steering attitude model used by GNSS satellites. In this early study, we use a box-wing satellite model for computational efficiency, though an arbitrary triangulated shape model can be used. A BRDF consisting of diffuse and specular components is used for the satellite surface.

We assume a diffusely reflecting Earth with a two-component surface albedo. The albedo in the polar

regions is varied. A range of albedo values is studied, covering annual variation and conceivable future changes. The changes in orbits are charted as a function of the albedo and orbital plane (relative to the solar direction).

3 Conclusions

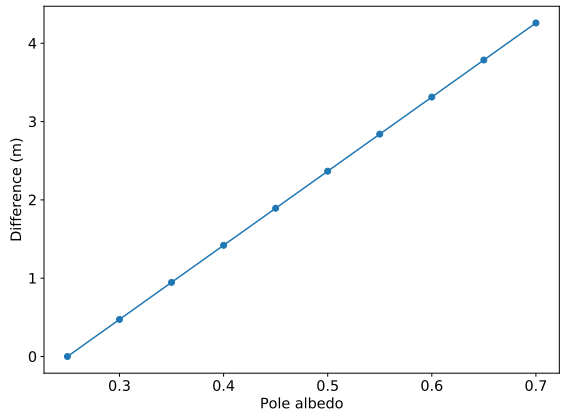

Figure 1: Relative displacement of the satellite after one orbit as a function of polar albedo, while the mid-latitude albedo is held constant at 0.25.

We find that under the influence of only the Earth-reflected radiation pressure, there is a clear linear relationship between the Earth's albedo and a displacement in the satellite's position after one orbit (Figure 1). This change is in the tens of centimetres range for albedo variations of 1%. These kinds of changes are theoretically detectable with modern SLR systems. The main caveat is that the other perturbative forces, particularly the Solar radiation pressure, must be modelled well enough to separate the Earth radiation pressure clearly. These are still areas of improvement in this modelling.

These results suggest that inversion of the global reflected radiation flux from changes to the orbits in a constellation of GNSS satellites is feasible.

Acknowledgements

This work is supported by the Academy of Finland.

References

[1] Rodriguez-Solano, C. J., Hugentobler, U., Steigenberger, P., Lutz, S.: Impact of Earth radiation pressure on GPS position estimates, J Geod 86:309–317, 2012.

[2] Montenbruck, O., Steigenberger, P., Hugentobler, U.: Enhanced solar radiation pressure modeling for Galileo satellites, J Geod 89:283–297, 2015.

[3] Montenbruck, O., Gill, E.: Satellite Orbits, Springer, 2000.

EPSC Abstracts
Vol. 11, EPSC2017-668, 2017
European Planetary Science Congress 2017

Low-temperature serpentinization reactions can explain molecular hydrogen production on Saturn's moon Enceladus: implications for potential microbial life

R.-S. Taubner (1,2), J. Zwicker (3), D. Smrzka (3), W. Bach (4), S.K.-M.R. Rittmann (1), C. Schleper (1), J. Peckmann (3,5)

(1) Archaea Biology and Ecogenomics Division, University of Vienna, 1090 Vienna, Austria, (2) Institute for Astrophysics, University of Vienna, 1180 Vienna, Austria, (3) Department of Geodynamics and Sedimentology, University of Vienna, 1090 Vienna, Austria, (4) MARUM Center of Marine and Environmental Sciences, 28359 Bremen, Germany, (5) Institute for Geology, University of Hamburg, 20156 Hamburg, Germany (ruth-sophie.taubner@univie.ac.at)

Abstract

The findings of the last decades that icy moons may harbor a large amount of liquid water under their ice shells have opened new horizons in the emerging field of Astrobiology. Several aspects have to be ascertained to determine if the subsurface aquifer of a certain celestial body may be able to harbor life-as-we-know-it. Here we focus on water-rock interaction processes during low-temperature serpentinization (T< 100°C) as potential source for hydrogen (H_2) production on Saturn's icy moon Enceladus. H_2 can serve as a potential substrate for hydrogenotrophic methanogenic life on Enceladus. In the course of serpentinization, the metasomatic hydration of olivine and pyroxene produces various minerals including serpentine minerals, magnetite, brucite, and carbonates. H_2 production only occurs if ferrous iron within iron-bearing minerals is oxidized and incorporated as ferric iron into magnetite. The PHREEQC code was used to model the pH- and temperature-dependent dissolution of olivine and pyroxene to form serpentine, magnetite, and H_2 under pressure and temperature conditions that may exist on Enceladus. Various model setups were run to assess the influence of environmental parameters on H_2 production. The combined results offer a constraint on H_2 production over time, and may aid habitability assessments of extraterrestrial bodies where serpentinization could occur.

Acknowledgements

We would like to thank David Parkhust for helping with the PHREEQC code, and Silas Boye Nissen for his support in the initial attempts of the serpentinization modeling process.

EPSC Abstracts
Vol. 11, EPSC2017-935, 2017
European Planetary Science Congress 2017

Dynamo driven by a precessing planet with an inner core

R. Laguerre (1), D. Cébron (2), J. Noir (3), N. Schaeffer (2) and V. Dehant (1)
(1) Royal Observatory of Belgium, Brussels, Belgium
(2) Université Grenoble, Alpes, ISTerre, Grenoble, France
(3) INstitute fo Geophysics, ETH Zurich, Zurich, Switzerland

Abstract

Precession has been proposed as an alternative power source for planetary dynamos and principle of future dynamo experiments. Previous hydrodynamic studies suggested that precession can generate very complex flows in planetary liquid cores. Following the pioneering work of A.Tilgner [1], the dynamo effect is demonstrated numerically in precession driven flow in spherical shells for a wide range of control parameters. The mechanisms of hydrodynamic instability and the level of saturation of both kinetic and magnetic energy are investigated in details and compared to analytical models. First conclusions about the behaviour of the dynamo at low Ekman numbers and low magnetic Prandtl numbers are drawn.

References

[1] Tilgner, A.: Precession driven dynamos, Physics of Fluids, Vol. 17, pp. 034104, 2005.